Climatology and Interannual Variability in the Intensity of Synoptic-Scale Processes in the North Atlantic from the NCEP–NCAR Reanalysis Data

SERGEY K. GULEV

P. P. Shirshov Institute of Oceanology, RAS, Moscow, Russia, and Institut für Meereskunde, Kiel, Germany

THOMAS JUNG AND EBERHARD RUPRECHT

Institut für Meereskunde, Kiel, Germany

(Manuscript received 30 May 2000, in final form 9 October 2001)

ABSTRACT

North Atlantic synoptic-scale processes are analyzed by bandpassing 6-hourly NCEP–NCAR reanalysis data (1958–98) for several synoptic ranges corresponding to ultrahigh-frequency variability (0.5–2 days), synoptic-scale variability (2–6 days), slow synoptic processes (6–12 days), and low-frequency variability (12–30 days). Climatological patterns of the intensity of synoptic processes are not collocated for different ranges of variability, especially in the lower troposphere. Intensities of synoptic processes demonstrate opposite trends between the North American coast and in the northeast Atlantic. Although north of 40°N the intensity of ultrahigh-frequency variability and synoptic-scale processes show similar interannual variability, further analysis indicates that secular changes, and decadal-scale and interannual variability in the intensities of synoptic processes may not be necessarily consistent for different synoptic timescales. Magnitudes of winter ultrahigh-frequency variability are highly correlated with the intensity of synoptic-scale processes in the 1960s and early 1970s. However, they show little agreement with each other during the last two decades, pointing to the remarkable change in atmospheric variability over the North Atlantic in late 1970s. North Atlantic ultrahigh-frequency variability in winter is highly correlated with surface temperature gradient anomalies in the Atlantic–American sector. These gradients are computed from the merged fields of SST and surface temperature over the continent. They demonstrate a dipolelike pattern associated with the North American coast on one hand, with the subpolar SST front and continental Canada on the other. High-frequency variability and its synoptic counterpart demonstrate different relationships with the North Atlantic Oscillation. Reliability of these results and their sensitivity to the filtering procedures are addressed by comparison to radiosonde data and application of alternative filters.

1. Introduction

Climate variability associated with the North Atlantic Oscillation (NAO) impacts Europe and North America on timescales from several years to several decades (Hurrell 1996; Hurrell and van Loon 1997; Davis et al. 1997; Rodwell et al. 1999; Stephenson et al. 2000). The NAO index is defined by the difference between normalized sea level pressure (SLP) anomalies in the Azores high and Iceland low (Rogers 1984; Barnston and Livezey 1987; Hurrell 1995b). This index is a measure of the strength of the midlatitudinal westerlies over the North Atlantic. Previous research has addressed links between interannual variability in the North Atlantic midlatitudinal circulation with the sea surface temperature (SST) and heat flux anomalies that are evident on both interannual and quasi-decadal timescales (Bjerknes 1964; Wallace et al. 1992; Cayan 1992a,b; Deser and Blackmon 1993; Kushnir 1994; Battisti et al. 1995; Iwasaka and Wallace 1995; Halliwell and Mayer 1996). These studies were based on primarily monthly mean atmospheric parameters available from the Comprehensive Ocean–Atmosphere Data Set (COADS; Woodruff et al. 1998), or from similar archives for selected variables (Trenberth and Paolino 1980; Maechel et al. 1998).

However, atmospheric responses to ocean signals should be primarily evident in the intensities of synoptic processes. The North Atlantic large-scale pressure gradient (NAO index) reflects the intensity of the zonal flow, associated with the baroclinic instability of the atmosphere. Initially, the SST signal forces the atmospheric synoptic variability rather than the large-scale meridional pressure gradient. Zorita et al. (1992) used intramonthly statistics from the COADS Monthly Summary Trimmed Groups (MSTG) as an indicator of circulation changes. However, these statistics are strongly influenced by random observational errors and inadequate sampling and disagree with statistical estimates

Corresponding author address: Sergey Gulev, P. P. Shirshov Institute of Oceanology, 36 Nakhimovsky Ave., 117851 Moscow, Russia.
E-mail: gul@sail.msk.ru

computed from the Ocean Weather Stations (OWSs) data (Gulev 1997a). Cyclone counts (Alpert et al. 1990; Schinke 1993; Stein and Hense 1994; Serreze et al. 1997; Blender et al. 1997) also include inhomogeneities, which result from changing data coverage and analysis techniques (Agee 1991; Ueno 1993; von Storch et al. 1993a) and uncertainties in storm detection based on pressure maps.

Data from the National Centers for Environmental Prediction–National Center for Atmospheric Research (NCEP–NCAR) and the European Centre for Medium-Range Weather Forecasts (ECMWF) reanalyses (ERA) (Kalnay et al. 1996; Gibson et al. 1997) provide an excellent opportunity to study variations in synoptic activity at different scales. The intensity of atmospheric synoptic processes has been quantified by computing variances for selected ranges (usually from 2–3 to 6–8 days) associated with synoptic-scale transients in the North Atlantic (Robertson and Metz 1990; Branstator 1995; Hurrell 1995a, Rogers 1997), or through counting ''zonal'' and ''blocking'' days in model simulations (Liu and Opsteegh 1995). Less attention has been paid to analysis of different subranges of synoptic variability (Blackmon et al. 1984; Ayrault et al. 1995). The present study is focused on the climatology and interannual variability of the intensities of atmospheric processes at different synoptic scales in the North Atlantic midlatitudes using the 40-yr record from the NCEP–NCAR reanalysis (Kalnay et al. 1996). Our study will identify the features that are common for different scales. We will also determine whether there are differences in climatology and interannual variability of the intensity of atmospheric synoptic processes at different scales.

2. Data and methods

We use NCEP–NCAR reanalysis data (Kalnay et al. 1996) for the period 1958–98. This dataset represents an effort to produce dynamically consistent synoptic-scale resolution fields of the basic atmospheric quantities and computed parameters. The NCEP–NCAR reanalysis data are influenced of course by the model and interpolation procedures. Care must be taken when it is used for budget studies (Kalnay et al. 1996). Da Silva and White (1996) and White (1999) found time-dependent imbalances in the global heat and moisture budget. We used SLP, winds, and geopotential heights, which in general are the most reliable fields. NCEP–NCAR reanalysis provides all parameters at 6-hourly temporal resolution and a $2.5° \times 2.5°$ spatial resolution (surface flux parameters are available at the so-called Gaussian grid of $1.875° \times \approx 1.9°$.) Pressure-level data as well as surface data are considered to be instantaneous values at the reference time. We have selected the area from the equator to 70°N and from 100°W to 30°E, which covers the North Atlantic and the adjacent continents.

To quantify the intensity of synoptic processes on the basis of 6-hourly data, we have applied bandpass filters. Wallace et al. (1988) argued that the characteristics of synoptic transients are in general insensitive to the use of different high-pass filters. On the other hand, filtering creates closer relationships between sequential values, and for our case (when several neighboring synoptic ranges are considered), the choice of the filtering procedure may be important. Rogers (1997) used polynomial filters. Ayrault et al. (1995) found Fourier filters to be effective for the identification of several synoptic ranges. Christoph et al. (1997) used a Murakami (1979) recursive filter for the bandpass of the National Meteorological Centre (NMC) analyses and European Centre–Hamburg Climate Model of the Max-Planck-Institut für Meteorologie (ECHAM) simulations. Hurrell (1995a) implemented the bandpass filter, which was evaluated by Trenberth (1991) for studying storm tracks in the Southern Hemisphere. For our task good spectral characteristics are required. To bandpass the synoptic time series, we used a Lanczos filter (Lanczos 1956; Duchon 1979; Gulev 1997a), which provides a very effective cutoff of the selected frequency. It does create Gibbs oscillations, which have been reduced by the smoothing in the frequency range. This filter was successfully used by Hoskins and Sardeshmukh (1987) for bandpassing ECMWF analyses. In the appendix we analyze the sensitivity of some of our results to the choice of different filters.

Consideration of synoptic spectra for different parameters indicates multiscale synoptic variability (see Gulev 1997a). Figure 1 shows an example of the averaged winter spectrum of 500-hPa geopotential height at 55°N, 20°W, within the North Atlantic storm track area. Al-

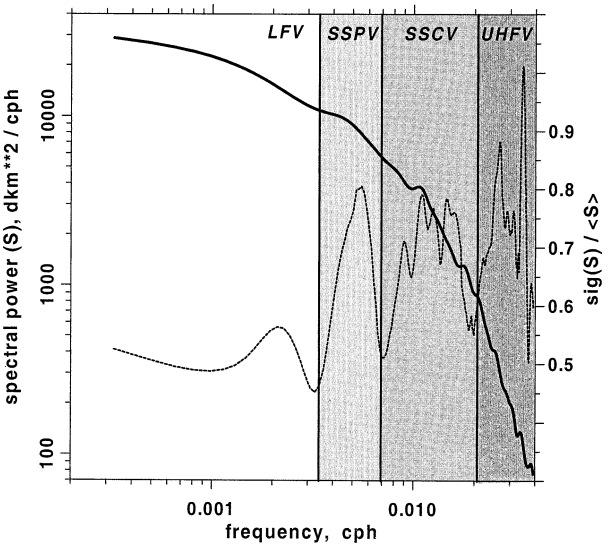

FIG. 1. Synoptic spectrum of 500-hPa geopotential height at 55°N, 20°W (bold line), averaged over 41 winters (1958–98), and normalized with respect to the averaged spectrum std dev of the spectral power (dashed line). Vertical lines show different ranges of synoptic and subsynoptic variability.

though for individual years some spectral peaks can be evident, averaging over primarily zonal and blocking winters results in the quasi-monotonous averaged spectrum. The standard deviations (std dev) of the spectral power, normalized with respect to the averaged spectrum (Fig. 1), shows that the largest interannual variability is associated with the periods 8–9, 3–5, and 0.5–1.5 days. Thus, we studied four ranges of variability: from 6 h to 2 days [ultrahigh-frequency variability (UHFV)], from 2 to 6 days [synoptic-scale variability (SSCV)], from 6 to 11 days [the so-called slow synoptic processes (SSPV)], and from 11 to 30 days [low-frequency variability of the background flow (LFV)]. This breakdown agrees with results from Ayrault et al. (1995) and Blackmon et al. (1984). The range from 2 to 6 days is associated with storm track variability (Ayrault et al. 1995; Hoskins et al. 1983; Hoskins and Sardeshmukh 1987; Wallace et al. 1988), although many authors (Trenberth 1991; Hurrell 1995a; Rogers 1997; Christoph et al. 1997) assessed storm track variability over the midlatitudes using a somewhat wider range (2–2.5 to 8 days), which may include the SSPV. For each of the four timescales, we performed bandpass filtering, and then computed the std dev of the bandpassed data. These std dev's were then used as measures of the intensity of synoptic processes within each band. Bandpassing of monthly series that are quite short does not effectively filter out all selected synoptic scales. Thus, we performed the analysis for seasonal series [January–March (JFM), April–June (AMJ), June–September (JAS), October–December (OND)] for every calendar year from 1958 to 1998. The use of the Lanczos window resulted in the 20-day cutoff of the 90-day time series. In order to avoid the influence of the seasonal cycle on the three monthly time series, third-order polynomial trends were removed before the bandpassing. Synoptic statistics were computed for geopotential heights at 1000, 850, 700, 500, and 300 hPa, for the thickness of 1000–500-hPa layer, and for some surface parameters.

3. Climatology of synoptic variability in the North Atlantic region

Figure 2 shows the std dev for different scales of synoptic variability of the 500-hPa geopotential height. All scales show pronounced annual cycles with the strongest variances in winter (JFM). The winter maximum of SSCV is located over Newfoundland and Nova Scotia and characterized by std dev values 6–6.5 dam. As predicted by Ayrault et al. (1995), the location of the UHFV maximum is shifted downstream from the SSCV maximum by approximately 800–1000 km. Maximum winter std dev of UHFV (2.5–2.8 dam) is less than half the std dev of SSCV. The intensity of SSPV is of the same order of magnitude as for the SSCV. The maximum of SSPV is displaced by about 700 km north of the maximum of SSCV. This shift is especially pronounced in the central midlatitude Atlantic. Low-frequency variability (Fig. 2g) is nearly twice as large as SSCV and SSPV, and has pronounced local maxima in the Canadian Archipelago, central midlatitude Atlantic, and Scandinavia.

For summer (Fig. 2d) the std dev at all synoptic scales are 1.5–2 times smaller than for winter. The largest relative seasonal changes are observed for the UHFV and SSCV. Although the locations of intensity maxima associated with the main North Atlantic storm track are similar for two seasons, there is a winter to summer shift of the midlatitudinal maxima of the std dev of UHFV and SSCV from the south to the north in the western Atlantic and from the north to the south in the eastern part. During summer, maxima of UHFV and SSCV in the North Atlantic storm track area align more zonally than for the winter season. There is also a shift of maxima of UHFV and SSCV from the offshore regions of the American coast to the open ocean from the winter to the summer season. Midlatitudinal maxima of SSCV and UHFV are more collocated during the summer and spring months, when the downstream shift of UHFV varies from 200 to 400 km. During winter and autumn this shift is much more pronounced (600–900 km). For the SSPV the pronounced winter maximum along the North American coast disappears in summer when the largest values are observed in the central midlatitudinal Atlantic. Winter to summer changes in the intensity of low-frequency variability are also characterized by the west–east shift of the maximum (Figs. 2g,h).

Figures 3a–c show the locations of winter maxima of the UHFV, SSCV, and SSPV for the 1000-, 700-, and 300-hPa levels. The downstream shift in the locations of the UHFV maximum with respect to the maximum of SSCV is mostly pronounced near the sea surface (1000 hPa) in wintertime (900–1200 km). Analysis of the SLP fields (not shown) reveals a somewhat larger shift between SSCV and UHFV (1200–1300 km). Recently Hoskins and Hodges (2002) examined bandpassed ERA SLP for the ranges 1–2 and 2–6 days. They found a shift from 800 to 900 km between the corresponding maxima of variances. At 300 hPa, the shift between SSCV and UHFV is less pronounced ($\approx$500 km). In the lower troposphere (1000–500 hPa) there are considerable differences in the location of maxima of SSCV and SSPV. The latter maximum is aligned nearly zonally at 60°N in the northeast Atlantic. At 300 hPa, maxima of SSCV and SSPV are nearly collocated over the North American coast and Newfoundland basin. Figure 4 shows the meridional sections of the intensity of UHFV, SSCV, and SSPV in the northeast Atlantic along 20°W during the winter and summer seasons. Remarkably for both winter and summer the minimum of variability at all synoptic scales is within the 850–700-hPa layer. The storm track at these levels is shifted northward with respect to the near-surface and upper levels. This is most pronounced for UHFV and SSCV during winter. During summer, storm track locations at different levels are much more consistent.

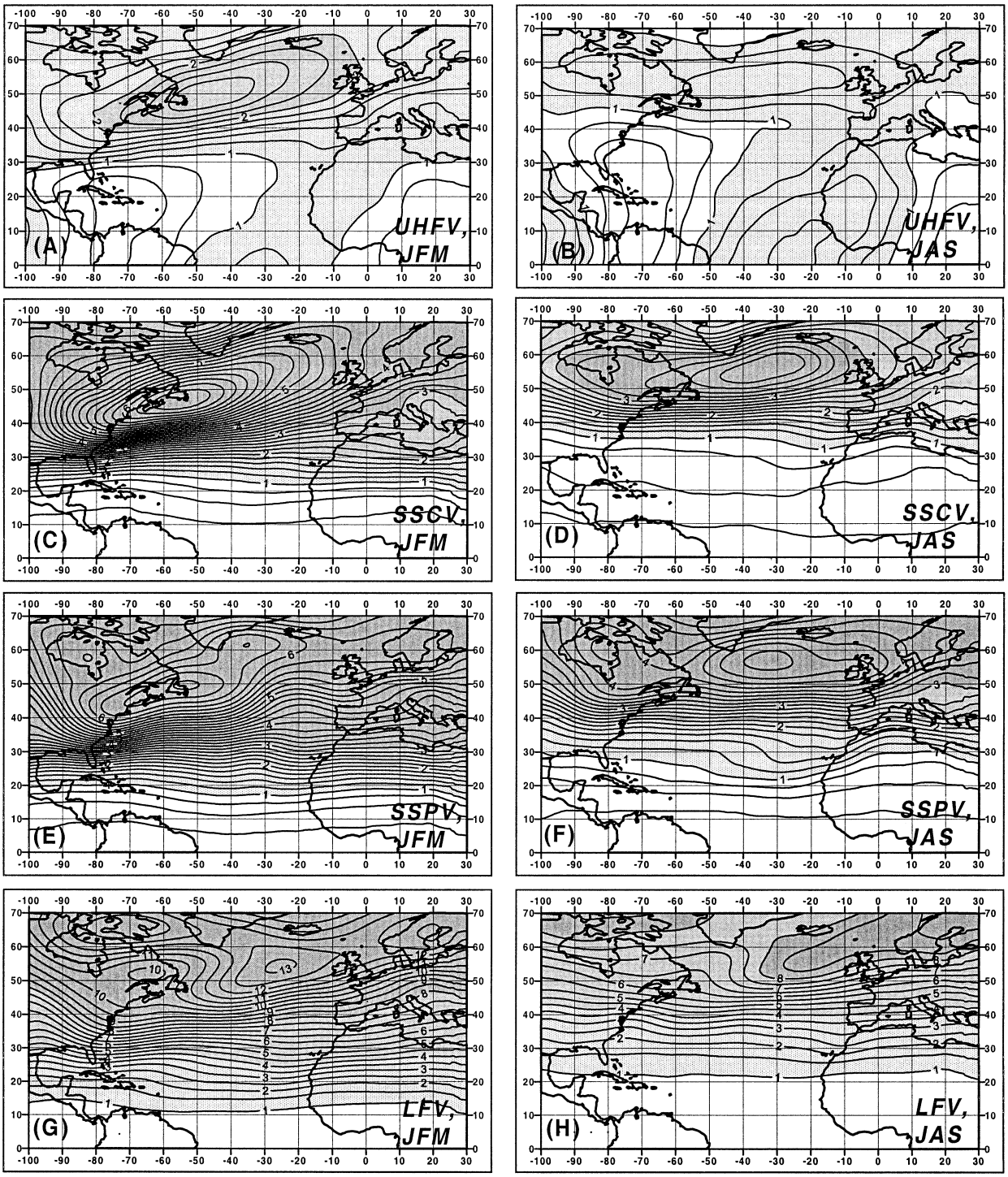

FIG. 2. Climatological std dev (dam) for different scales of synoptic variability of 500-hPa geopotential height: UHFV for (a) winter and (b) summer, SSCV for (c) winter and (d) summer, SSPV for (e) winter and (f) summer, LFV for (g) winter and (h) summer.

The maximum of SSCV associated with the North Atlantic storm track is shifted downstream and poleward of the climatological jet stream identified by the winter (JFM) mean 250-hPa zonal wind component in Figs. 3a–c, consistent with the growing intensity of baroclinic waves downstream of the areas of enhanced baroclinicity (Simmons and Hoskins 1978). The winter maximum of SSCV at 500 hPa (Fig. 2) exhibits a zonal shift of 25° and a meridional shift of 10° that corresponds in general to the results of Christoph et al. (1997) based

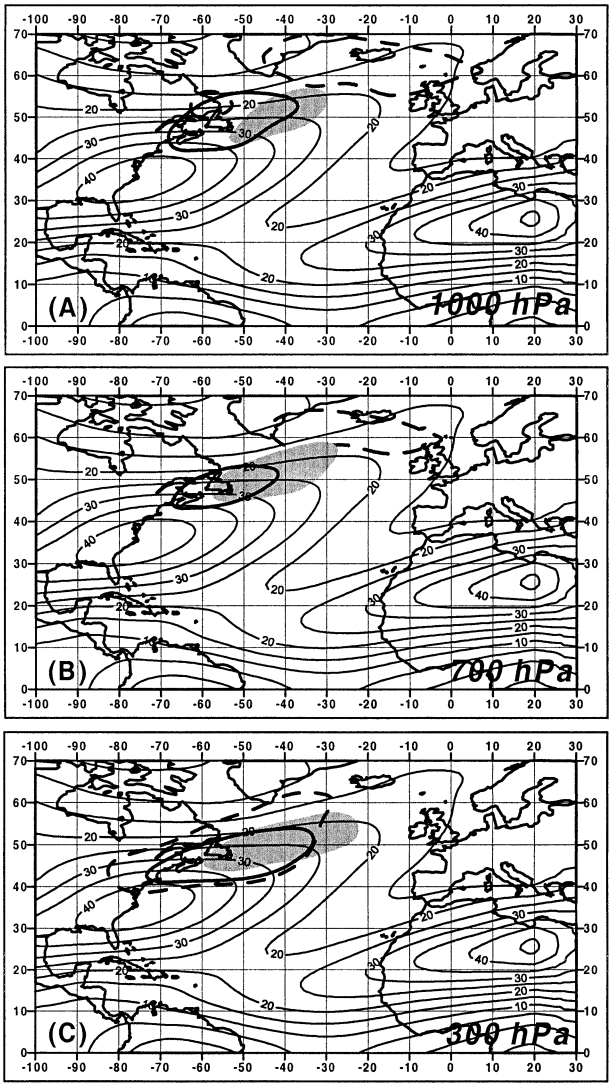

FIG. 3. Locations of maxima of UHFV (bold contour), SSCV (shading), and SSPV (dashed contour) for (a) 1000-, (b) 700-, and (c) 300-hPa levels, overplotted by 250-hPa zonal wind velocity (m s^{-1}). Contours of maxima correspond to the 90% of maximum values of std dev.

on operational NMC analyses from the late 1960s to the late 1980s.

4. Linear trends in the intensity of synoptic processes

First we consider secular changes in the intensity of different synoptic processes for the period from 1958 to 1998. The NAO index indicates pronounced upward changes from primarily negative values in the 1960s to primarily positive values during the 1980s and 1990s (Hurrell 1995b). Figure 5 shows estimates of linear trends in the intensity of atmospheric synoptic processes for winter together with their statistical significance (*t* test). In the area of the main North Atlantic storm track there is a tendency for intensification of synoptic and subsynoptic variability at all pressure levels. The area of pronounced positive trends in the intensity of UHFV in the northeast Atlantic also extends over northern Europe. Trends in the UHFV range from 0.1 to 0.3 dam $decade^{-1}$. For SSCV and SSPV significantly positive trends are shifted to the west. The most pronounced upward trends are found in the midlatitudinal central and west Atlantic and range from 0.3 to 0.7 dam $decade^{-1}$. SSCV shows significantly positive trends over the northern North America, not present in the UHFV.

The relative contribution of linear trends to the total variability, estimated as ratios between trend-only and the total std dev, vary in space from 0.1 to 0.4, but is constant with height. This allows us to compare trend magnitudes at different levels. There are somewhat stronger trends at all timescales for the upper levels in comparison to the planetary boundary layer. Positive linear trends in the intensity of SSCV at 1000 hPa are less than 0.2 dam $decade^{-1}$ and significant only southwest of Iceland. By contrast, SSCV trends at 500 hPa (Fig. 5d) are significant over the whole midlatitudinal North Atlantic. If we consider secular changes in the thickness of the 1000–500-hPa layer (Figs. 5g,h), trends in SSCV are positive along the whole North Atlantic storm track and show a more coherent pattern than seen in the SSCV of 500-hPa geopotential height. Thus, the SSCV over the storm track is enhanced primarily due to the variations in the thickness of the 1000–500-hPa layer rather than because of barotropic changes. Local maxima of the largest positive trends in UHFV and especially in SSCV are shifted to the west in comparison to the 500-hPa level.

In the region along the North American coast, there are significant negative trends from -0.08 to -0.15 dam $decade^{-1}$ for UHFV and from -0.1 to -0.2 dam $decade^{-1}$ for SSCV (Fig. 5). Negative trends in SSPV are less pronounced than for synoptic-scale and UHFV at the 500-hPa level (Fig. 5e). Negative linear trends over the North American coast in UHFV are strongest near the sea surface, and for SSCV are mostly pronounced at the 500-hPa level. This is the so-called storm formation region (Sutton and Allen 1997). However, Fig. 5 shows different secular tendencies and does not support the hypothesis about the correlated changes of storm activity over the North American coast and in the northeast Atlantic, at least on a timescale of secular changes.

Another region with a substantial decrease in the intensity of synoptic and subsynoptic variability is the subtropical northeast Atlantic, the Iberian Peninsula, and the western Mediterranean. This region is traditionally associated with the Mediterranean cyclone mode, which is intensified under the dominance of the blocking regime and the intermediate ''Greenland anticyclone'' (GA) regime, when the midlatitudinal flow is shifted to the south (Hannachi and Legras 1995; Ay-

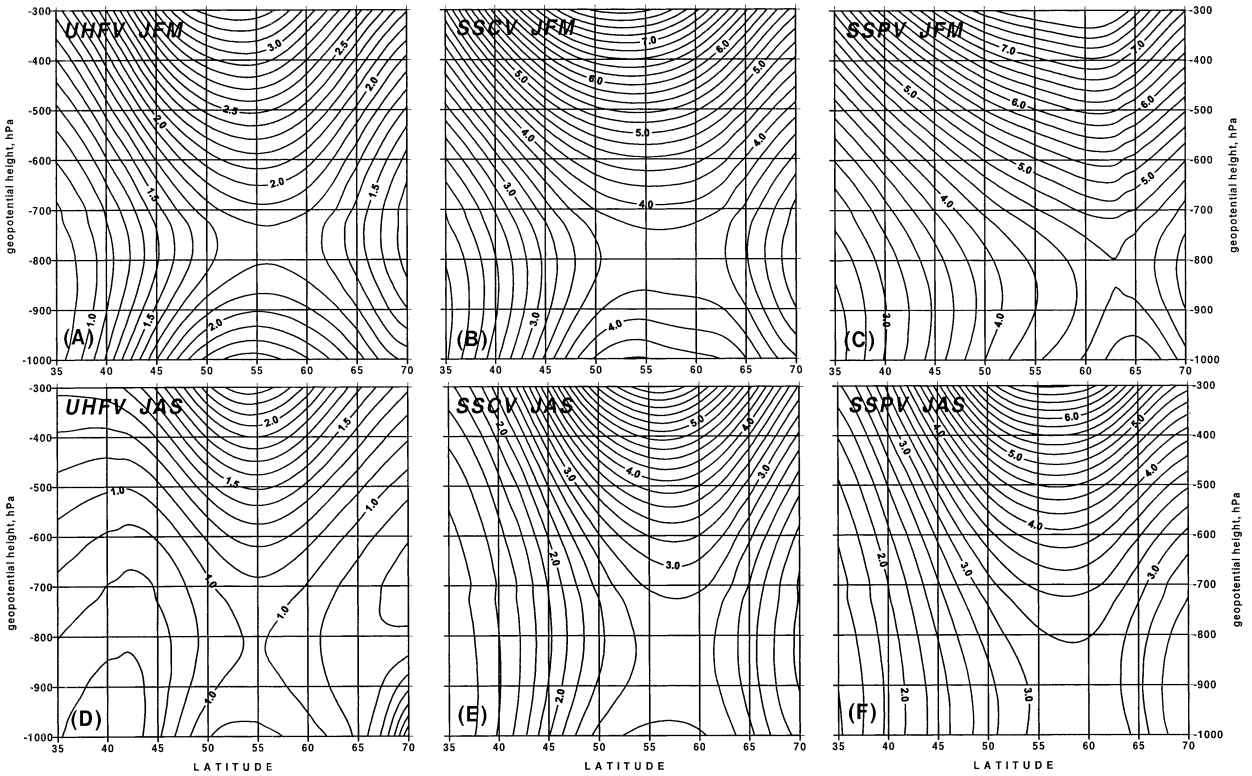

FIG. 4. Meridional sections along 20°W of the intensity of (a),(d) UHFV, (b),(c) SSCV, and (c),(f) SSPV for (a),(b),(c) winter and (d),(e),(f) summer seasons.

rault et al. 1995). Strengthening and weakening of both regimes are associated with primarily negative and positive NAO indices, respectively. Significantly negative trends in UHFV, SSCV, and SSPV over the eastern Mediterranean range from -0.08 to -0.15 dam decade^{-1}. Significant negative linear trends of 1000–500-hPa thickness over the North American coast and western Mediterranean are pronounced in both UHFV and SSCV (Figs. 5g,h).

Although the UHFV and SSCV trend patterns are quite similar, UHFV shows the largest secular changes in the central and northeast Atlantic. The largest changes in the SSCV occur in the northwest Atlantic and over North America. The spatial pattern of linear trends in SSPV differs from those for UHFV and SSCV. The area of increasing intensity of SSPV is restricted to the central North Atlantic. The area of negative changes over the American coast is smaller and shifted to the south. The area of negative trends expands to the Gulf of Biscay and the northeast Atlantic. Secular changes in the intensity of the LFV (Fig. 5f) exhibit tendencies opposite to those obtained for UHFV and SSCV. Significantly negative trends appear in the northeast Atlantic. The region over the North American coast is characterized by positive trends. LFV (12–30 days) depicts the frequency of the changes between different regimes of the circulation over the North Atlantic. Growing synoptic-scale variability in the storm track as expected corresponds to the decrease in the occurrence of blocking and Greenland anticyclone regimes over the northeast Atlantic.

5. Interannual variability in the intensities of synoptic processes

a. Changes in the spectral structure of synoptic variability

We computed synoptic spectra of different parameters for every winter (JFM) from 1958 to 1998 for a number of midlatitudinal locations in the area of the North Atlantic storm track. Averaging of the 41 individual winter spectra $S(\omega)$ results in the ''climatological'' spectrum $\langle S(\omega)\rangle$ (an example is given in Fig. 1), which is represented by a red-type smooth function. Then we derived anomalies of the spectral power at every frequency for every winter with respect to the climatological spectrum and normalized them by scaling with the interannual std dev of spectral power at each frequency:

$$S'(\omega, t) = [S(\omega, t) - \langle S(\omega)\rangle]/\sigma[S(\omega, t)]. \qquad (1)$$

Figure 6 shows the evolution of the normalized spectral anomalies of 500-hPa height, for the locations 37.5°N, 65°W and 55°N, 20°W. Spectral anomalies were smoothed with a 5-yr running mean, that results in the

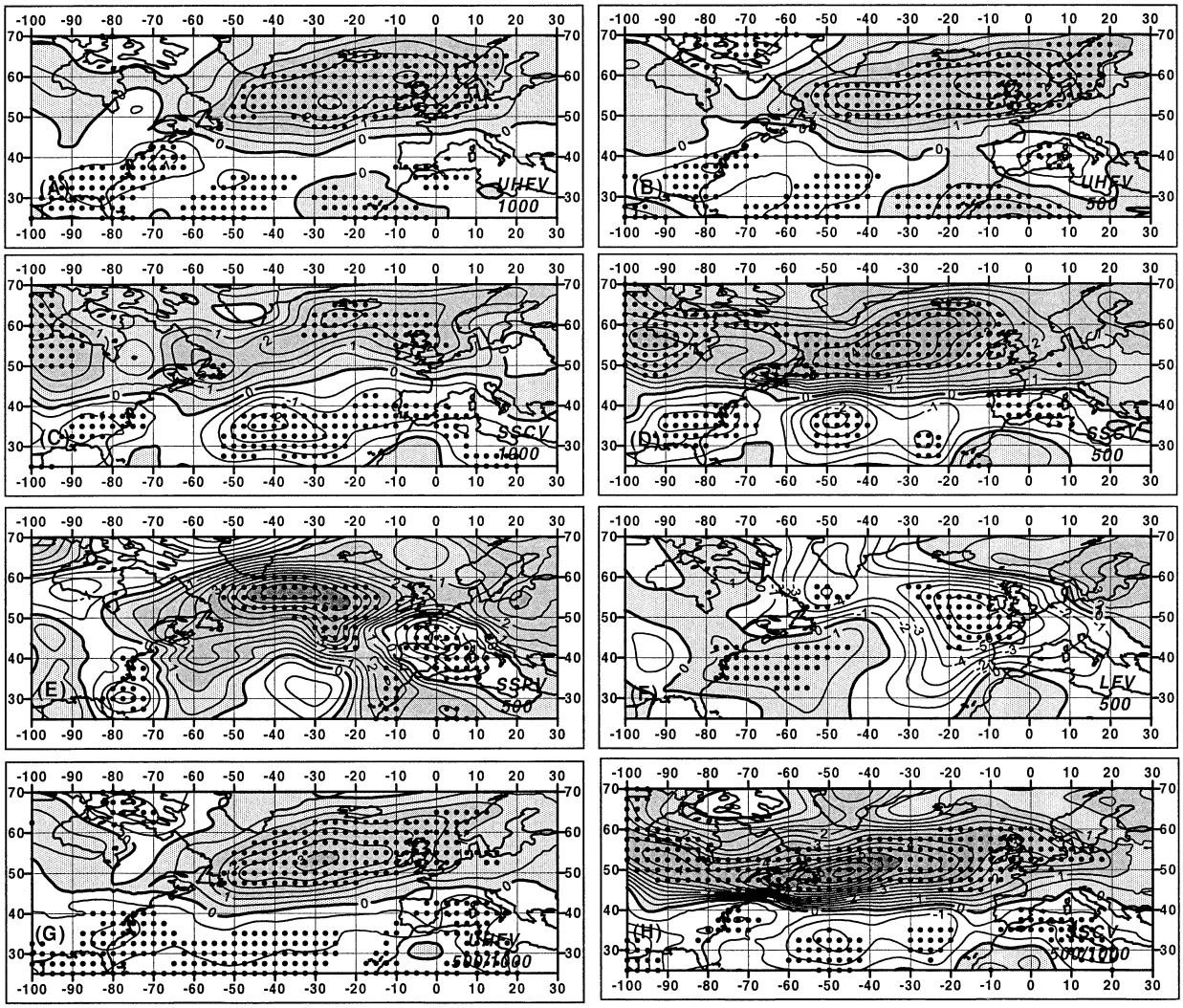

FIG. 5. Estimates of linear trends (dam decade^{-1}) in the intensity of UHFV at (a) 1000-hPa and (b) 500-hPa levels, SSCV at (c) 1000-hPa and (d) 500-hPa levels, (e) SSPV and (f) low-frequency variability at 500-hPa level, and (g) UHFV and (h) SSCV of the thickness of 1000–500-hPa level. Trends that are significant at 95% level (*t* test) are denoted by black circles. Shaded areas correspond to positive trends.

2-yr cutoff in the beginning and the end of the record. In the northwest Atlantic over the Gulf Stream there has been an intensification of the slow synoptic variability at the timescales from 5–6 to 12 days during the period from the early 1960s to the 1990s. At the same time, the range of UHFV and SSCV is characterized by primarily positive spectral anomalies during the 1960s and early 1970s and by negative anomalies for the 1980s and 1990s. In the late 1970s–early 1980s there was a switch from negative to positive anomalies in the low-frequency range, and an opposite change for the high-frequency range. The corresponding plot for the location in the northeast Atlantic (Fig. 6b) shows a pronounced tendency for enhancement of the UHFV and SSCV in the 1980s and 1990s in comparison to the 1960s and 1970s. Thus, the dominant synoptic processes became faster in the 1980s and 1990s. The intensity of synoptic processes at periods longer than 3 days also indicates pronounced quasi-decadal changes, especially in the northeast Atlantic. Thus, the structure of variability of the intensity of synoptic processes of different scales is quite different in the northeast and the northwest Atlantic. This agrees with the expected behavior of synoptic transients for the blocking and zonal events. During blocking regimes (low NAO index), synoptic-scale transients propagate into the northeast Atlantic, though the location of the track is shifted to the south and the UHFV is depressed. For the zonal regimes (high NAO index), there is an enhancement of the UHFV in the northeast Atlantic (Ayrault et al. 1995).

To examine variability from several years to two decades we selected the average winter position of the main North Atlantic track (Fig. 2), and computed spectra of interannual variations of synoptic intensities in

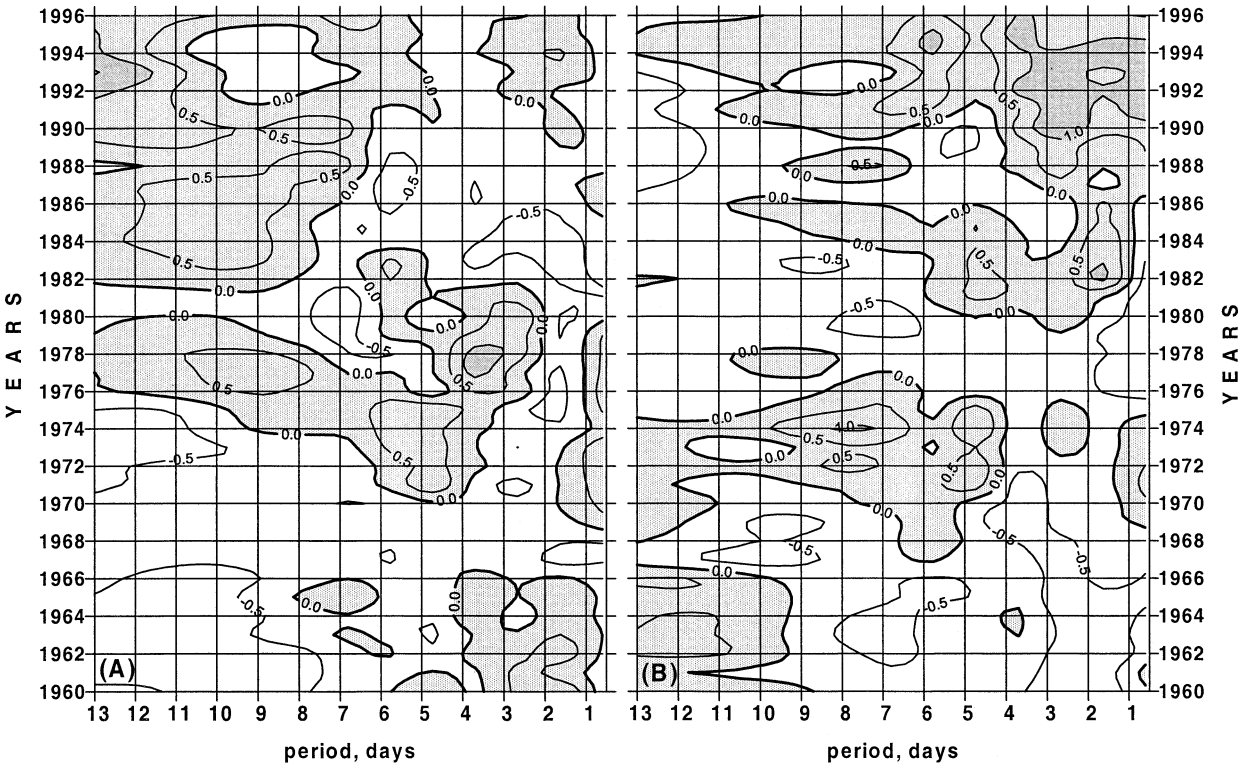

FIG. 6. Interannual evolution of the normalized and smoothed with 5-yr running mean spectral anomalies of 500-hPa height for the locations (a) 37.5°N, 65°W and (b) 55°N, 20°W.

every point of the line, corresponding to the latitudinal maximum of variance. Differences between the spectra computed for the 6 selected lines within the band ±2.5° latitude, are within the range ±10% of spectral power. Thus, for every point in the longitudinal direction we averaged spectra from the 3 latitudinal points, located 2.5° north and south of the central point. Figure 7 shows the evolution of the winter spectra of UHFV, SSCV, SSPV, and LFV of 500-hPa height along the selected storm track from the west to the east. For UHFV a 4–5-yr spectral maximum is pronounced along the whole storm track with the enhancement over the Great Lakes and in the region east of Newfoundland, where there is also a pronounced 2–3-yr spectral maximum. Longer-term variability is represented by 8–10-yr oscillations, which are pronounced only over the ocean. The 7–10-yr oscillations in the intensity of SSCV (Fig. 7b) are also pronounced over the ocean only. The location of the 7–10-yr spectral maxima for UHFV is shifted downstream with respect to SSCV by approximately 800–850 km. Interannual variability in the intensity of SSPV (Fig. 7c) is characterized by periods of 7–9 yr, pronounced over North America and northern Europe. The North Atlantic storm track area is characterized by relatively weak variability at 4–5 yr in the western and eastern parts. Variability in the intensity of the LFV is pronounced over the North Atlantic midlatitudes (Fig. 7d) and exhibits the enhancement of spectral power at 3 yr and 8–12 yr in the northwest Atlantic and at somewhat longer periods (10–16 yr) in the northeast Atlantic.

b. EOF analysis of interannual variability of synoptic intensities

To depict spatial patterns associated with variability at different timescales, we applied empirical orthogonal function (EOF) analysis to the winter anomalies of the intensity of synoptic processes. Figure 8 shows the first two EOFs of the UHFV (Figs. 8a,b) and SSCV (Figs. 8c,d) variability. For UHFV (SSCV) the first two EOFs account for 36% (30%) and 22% (18%) of the total variance, respectively. Figure 9 summarizes the time behavior of the corresponding normalized principal components (PCs). The first EOF shows the variations in the strength of the North Atlantic midlatitudinal storm track associated with the NAO. Centers of action for both UHFV and SSCV are associated with the midlatitudinal northwest Atlantic and the western subtropics. This corresponds to midlatitude and polar cyclogenesis and weakening of cyclone generation near the American coast. The second EOF captures latitudinal shifts of the storm track. Only the second normalized PCs of the UHFV and SSCV are highly correlated with each other ($r = 0.78$). For the first PCs the correlation between the UHFV and SSCV is lower ($r = 0.64$). The correlation

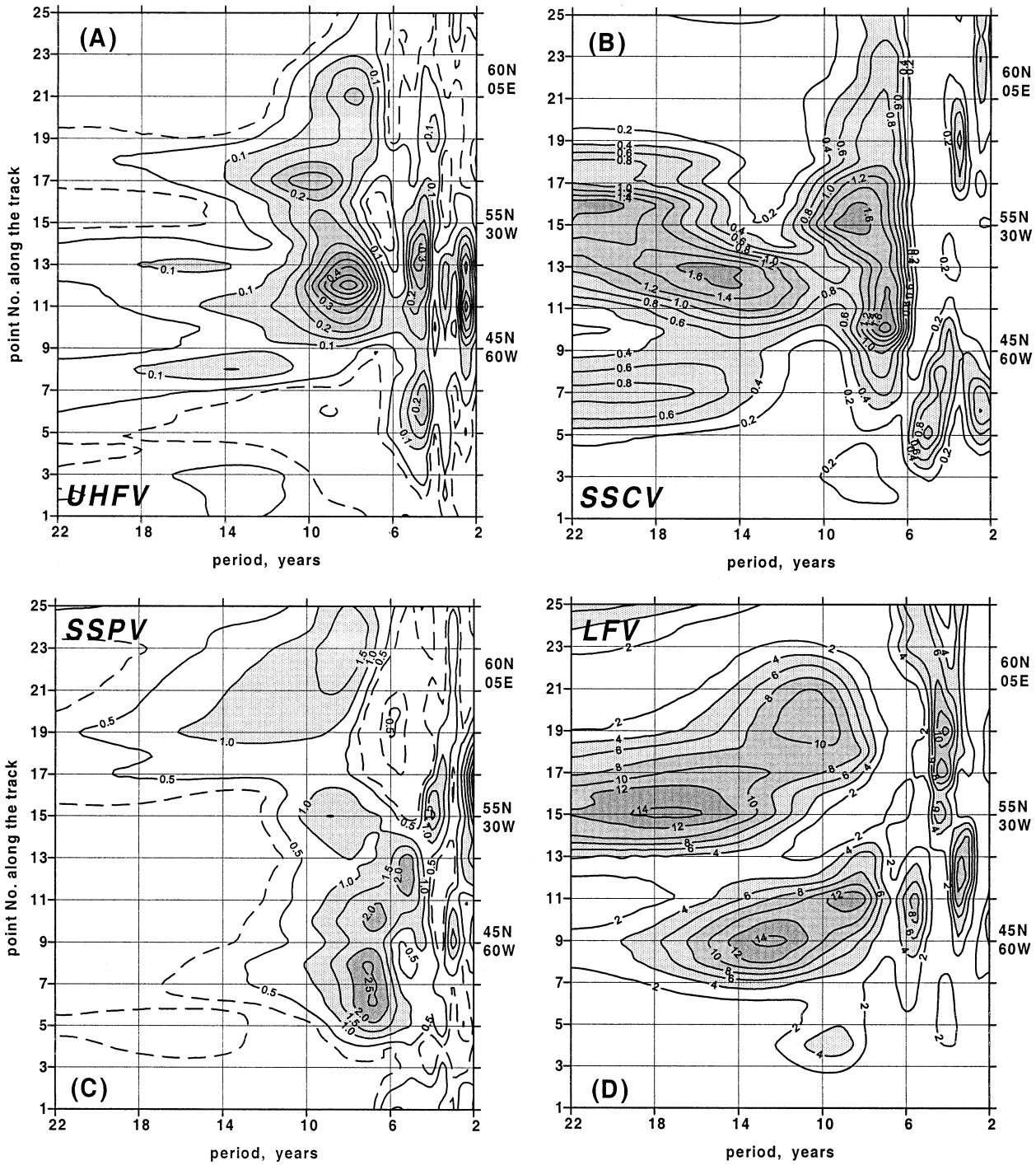

FIG. 7. Evolution of the spectra of (a) UHFV, (b) SSCV, (c) SSPV, and (d) low-frequency variability along the midlatitudinal storm track in the North Atlantic. Spectral power is in dam^2 (cpy)$^{-1}$.

between the first PCs of UHFV and SSCV for the period 1958–77 is considerably larger than for 1978–98 (0.75 and 0.48, respectively). This break coincides in time with the sharp change in the spectral structure of synoptic variability (Fig. 6).

To analyze modes of variability in the mean fields associated with the intensity of synoptic processes, we computed canonical correlations between SLP and the intensity of UHFV and SSCV. Canonical correlation analysis (CCA; von Storch and Zwiers 1999) is widely used in climate research for identifying linked modes of different parameters (Zorita et al. 1992; von Storch

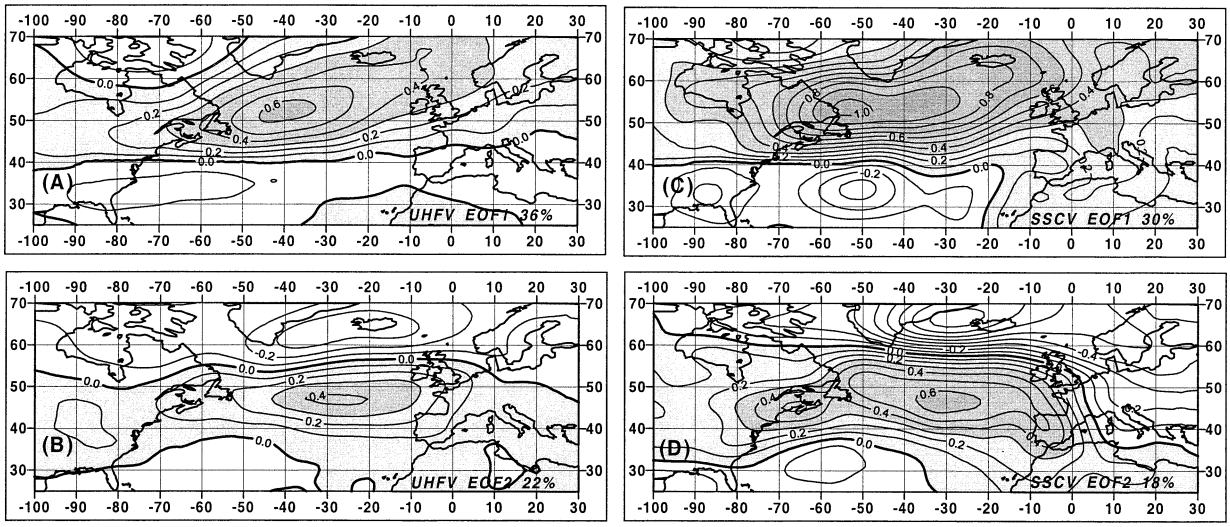

FIG. 8. (a),(c) First and (b),(d) second EOFs of the anomalies of geopotential height of 500-hPa level for (a),(b) UHFV and (c),(d) SSCV.

et al. 1993b; Heyen et al. 1996; others). The first five EOFs (78%, 75%, and 80% of the total variance in UHFV and SSCV and SLP, respectively) were used for the CCA. Results remain very stable for the range of truncation from the first 3 to 7 EOFs. Figure 10 shows patterns of the first two canonical pairs UHFV–SLP and SSCV–SLP. The first two CCA pairs between UHFV and SLP are correlated at 0.91 and 0.85, respectively. Corresponding correlation coefficients for the SSCV and SLP are 0.90 and 0.83. The pattern of the UHFV of the first CCA pair (Fig. 10a) resembles the first EOF, shown in Fig. 8a. The corresponding SLP pattern is the NAO pattern made by the Azores high and the Iceland low (Fig. 10b). The second pair's UHFV pattern (Fig. 10e) shows intensification of subsynoptic processes in the vicinity of the North American coast associated with the weakening of the midlatitudinal UHFV. The corresponding SLP pattern (Fig. 10f) reflects intensification of the meridional circulation regimes, which may influence the southward shift of the midlatitudinal storm track. This SLP pattern was identified earlier by Glowienska-Hense (1990). If we consider the canonical patterns for the SSCV, the first pair (Figs. 10c,d) reflects the intensified synoptic-scale variability in the midlatitudinal northwest Atlantic and in the northeast Atlantic high latitudes, associated with blocking in the Atlantic–European sector in the SLP field. Only the second canonical pair (Figs. 10g,h) demonstrates the NAO-like pattern in the SLP and associated strengthening of the North Atlantic storm track. Thus, although north of 40°N, increased westerlies are highly correlated with a stronger storm track for both UHFV and SSCV, the EOF analysis demonstrates some differences in the time behavior of the SSCV and its high-frequency counterpart, and shows that the dominant modes of UHFV and SSCV may be associated with different patterns in the mean SLP fields.

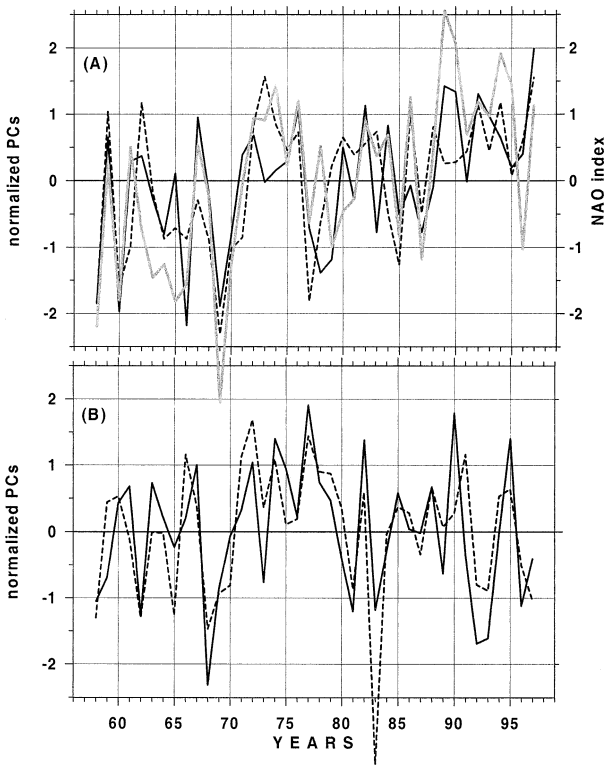

FIG. 9. (a) First and (b) second normalized principal components of the geopotential height of 500-hPa level for UHFV (solid line) and SSCV (dashed line). Bold gray line in (a) corresponds to the NAO index.

c. *Intensities of atmospheric synoptic processes and the North Atlantic Oscillation*

The CCA analysis demonstrates that links between the NAO and the intensity of atmospheric synoptic var-

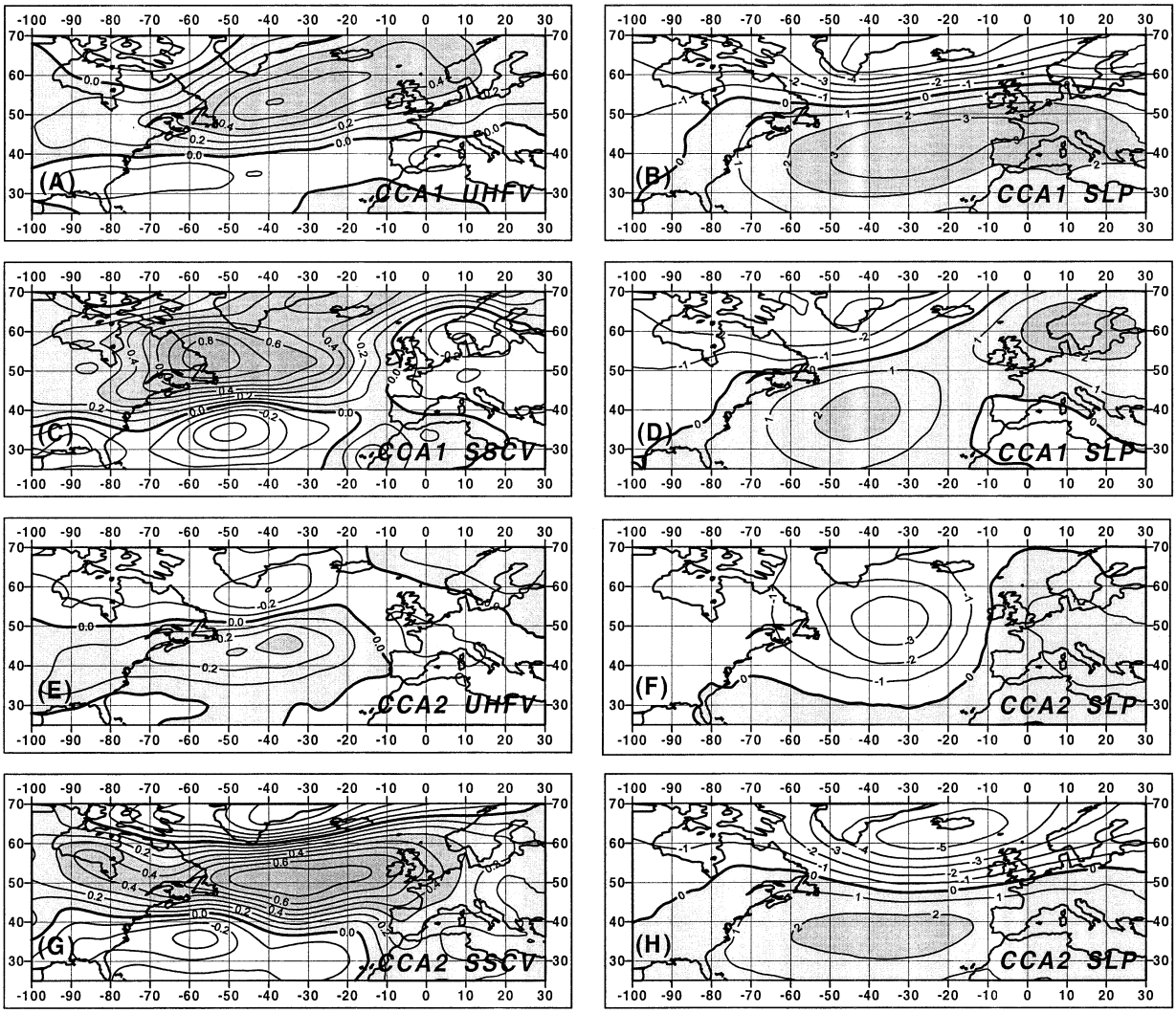

FIG. 10. (a–d) First and (e–h) second canonical patterns for (a),(e) UHFV and (b),(f) SLP and for (c),(g) SSCV and (d),(h) SLP.

iability at different timescales are more complicated than the traditionally assumed pattern of intensification and weakening of the midlatitudinal storm track. Using rotated EOFs, Rogers (1997) found that the North Atlantic storm track pattern is linked to the SLP dipole centered over the Bay of Biscay and the Barents Sea rather than to the NAO index. In this context the shift of the NAO dipole to the east in the late 1970s described by Hilmer and Jung (2000) may explain decreasing correlation between the NAO and storm track activity in the North Atlantic for the last two decades. Remarkably, the first PCs of UHFV and SSCV (Fig. 9a) exhibit much higher correlation with the NAO index for the period 1958–77 (0.81 and 0.77, respectively) than for the last two decades (0.61 and 0.41, respectively). Figure 11 shows associated correlations between the NAO index and the intensities of UHFV and SSCV. For the whole 41-yr period (Figs. 11a,b) there are differences in the correlation patterns for UHFV and SSCV. UHFV demonstrates the highest correlations over the midlatitudinal storm track and over northern Europe. Negative correlations are found over the east coast of North America, the subtropical Atlantic, and southern Europe. For SSCV the area of high positive correlations extends to central and southern Europe. Correlations for the periods 1958–77 (Figs. 11c,d) and 1978–98 (Figs. 11e,f) demonstrate remarkable differences. Correlations between the NAO and UHFV are slightly higher for the first period in the central Atlantic, but are higher for the second period in the eastern Atlantic and over northern Europe. For SSCV, significantly positive correlations for the period 1958–77 align across central and southern Europe (as for the Greenland anticyclone regime). For the last two decades, SSCV is positively correlated with the NAO index in the northeast Atlantic and over northern Europe, but it is negatively correlated over the Mediterranean.

Kodera et al. (1999) assumed that the NAO index

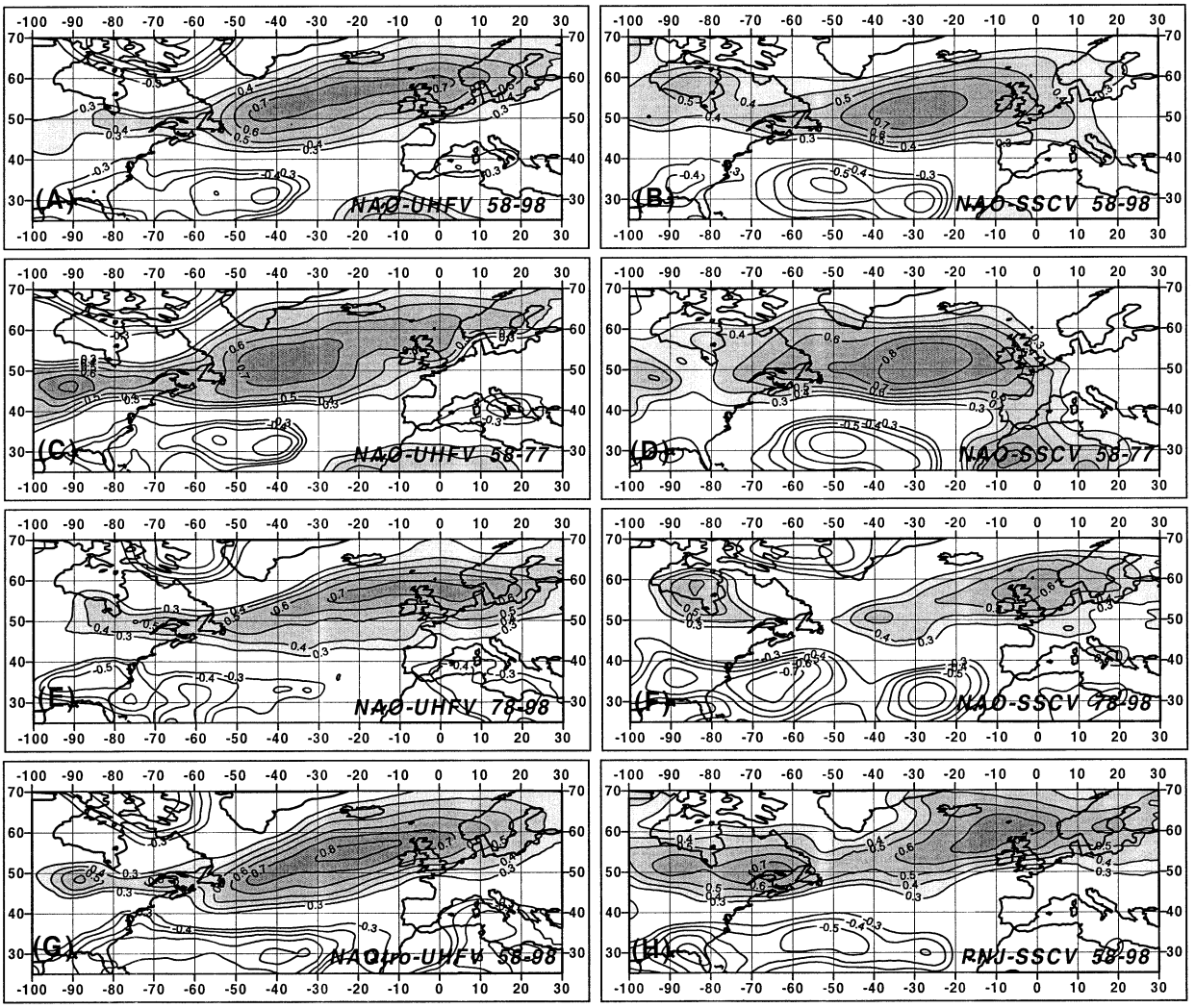

FIG. 11. Associated correlations of the NAO index with (a),(c),(e) UHFV and (b),(d),(f) SSCV for the periods (a),(b) 1958–98, (c),(d) 1958–77, (e),(f) 1978–98, associated correlations between the tropospheric NAO index and UHFV of the thickness of (g) 1000–500-hPa layer, and (h) between the PNJ index and SSCV for the period 1958–98.

includes the joint effects of local North Atlantic–European variability and a hemispheric mode, associated with the intensity of the polar night jet (PNJ) in the lower stratosphere. Normalized anomalies of zonally averaged 50-hPa zonal wind at 65°N can be used as a PNJ index, which is closely correlated with the Arctic Oscillation (Thompson and Wallace 1998). The regional tropospheric mode can be characterized by a tropospheric NAO index, which can be derived as $NAO_{tro} = NAO - r(PNJ)$, where r is the correlation coefficient between the NAO and PNJ indices (Kodera et al. 1999). We evaluated PNJ and NAO_{tro} indices using upper-layer NCEP–NCAR wind data for winter. The correlation coefficient between the NAO and PNJ for 1958–77 is 0.43 and grows for the period 1978–98 to 0.64 in agreement with Kodera et al. (1999). Figure 11g shows the correlation between the NAO_{tro} and UHFV of the thickness of the 1000–500-hPa layer for the period 1958–98. Figure 11h shows the correlations between the PNJ index and SSCV for the same period. The pattern in Fig. 11g is comparable with that in Figs. 11c,e and demonstrates even higher positive correlations over the midlatitudinal storm track zone. SSCV is highly correlated with the PNJ over the last four decades in the northeast Atlantic and over the North American continent. Thus, during the period 1958–77, when the NAO was largely influenced by the tropospheric mode, SSCV was closely related to the NAO in the storm track area aligned across central and southern Europe. Northern Europe was primarily under the influence of the fast synoptic transients represented by UHFV and correlated with the surface temperatures in the northwest Atlantic and over the American continent. During the last two decades, when NAO was also under the influence of the hemispheric mode, SSCV showed the pattern over northern Europe driven by PNJ variability. The results in Fig. 11, can

be influenced by secular trends in the time series, associated with the changes in the data assimilation input (White 1999). Correlations computed after removing trends from the intensities of synoptic variability and from the indices time series (not shown) are very similar to those displayed in Fig. 11. Although there was a slight decrease (0.02–0.08) in the correlation coefficients for the 41-yr time series, these are not statistically significant. For the shorter 20-yr periods, changes are considerably smaller and spatial patterns nearly coincide with each other. There is a small increase in the correlation between SSCV and the NAO and PNJ indices for both periods.

6. Relationships between the intensity of synoptic processes and surface temperatures

Prior work has demonstrated close relationships between the leading modes of the atmospheric circulation and SST in the North Atlantic Ocean (Wallace et al. 1990; Hense et al. 1990; Zorita et al. 1992; Deser and Blackmon 1993; Kushnir 1994; Peng and Fyfe 1996; Halliwell 1997; Venzke et al. 1998; others). Usually, the dominant North Atlantic SST mode represents a dipole with the centers of action in the subpolar and subtropical gyres, which is associated with the NAO-like circulation pattern. This relationship has been found using different data, various observational periods, and different analysis procedures. This demonstrates the reliability of interaction between the atmospheric and oceanic modes. Wallace et al. (1990) suggested that the westerlies in the midlatitudes can be enhanced in the case of a positive anomaly of the subtropical SST. This idea was developed further by Kushnir (1994). Latif and Barnett (1994) proposed a mechanism for the North Pacific assuming a positive feedback driven by the SST anomalies and fluxes, and a negative feedback associated with the lagged response of the subtropical gyre to anomalous wind stress. Groetzner et al. (1998) studied this mechanism in the North Atlantic. Robertson et al. (2000), using NCEP–NCAR 500-mb mean heights and Global sea Ice and Sea Surface Temperature data (GISST) identified the North Atlantic leading interaction mode similar to that found by Groetzner et al. (1998).

Since the main SST pattern is associated with the subpolar–subtropical dipole, the SST gradient in the midlatitudes may serve as an effective characteristic of the SST signal. Harnack and Broccoli (1979) and Lanzante (1983) considered the possible impact of the meridional SST gradient in the North Pacific and North Atlantic midlatitudes on the midtropospheric circulation. In the North Atlantic the highest significant positive correlation between the SST gradients and zonal geostrophic winds was found for the belt 35°–45°N (Lanzante 1983). Lambert (1996) found significant positive correlations between the midlatitudinal North Pacific SST gradient and the number of intense cyclones in the Pacific, suggesting modulation of the atmospheric baroclinicity by the average SST gradients. Recently Geng and Sugi (2001) analyzed the role of the large-scale SST gradients in the changes of cyclone activity over the Atlantic. They found no evidence of the direct influence of the SST gradient on the cyclone activity. In these studies only large-scale SST gradients, computed from 10° and larger boxes, were considered. They are reasonably correlated with the intensity of the SST anomalies in the subtropical and subpolar gyre. However, changes in the baroclinic instability in the lower atmosphere in the northwest Atlantic are more influenced by smaller-scale gradients in the vicinity of the subpolar SST front, which may not be directly related to the large-scale pattern. Cyclogenesis over the North American coast is associated with sea–land temperature differences. Dickson and Namias (1976) first analyzed surface temperature gradients over the United States and found them to be strongly linked to the intensity of cyclogenesis on subtropical and subpolar fronts. Wallace et al. (1995) found an out-of-phase behavior of temperature anomalies over the land and the ocean. Recently Broccoli et al. (1998) analyzed a 1000-yr model run with a coupled ocean–atmosphere model and found the so-called cold ocean–warm land pattern to be one of the most pronounced features of climate variability in the Atlantic sector.

To investigate possible joint effect of SST gradients and sea–land temperature gradients we merged the Reynolds SST dataset (Smith et al. 1996) over the ocean with the NCEP–NCAR ground skin temperature over the land, and obtained the 41-yr fields of what we term ''surface temperature'' on a $2° \times 2°$ grid. Interpolation was accomplished by the method of local procedures (Akima 1970) separately for the SST and ground temperatures, and only then they were merged, that is, no interpolation across the coastline was applied. The resulting fields demonstrate effects of land–sea temperature differences as well as oceanic SST and continental surface temperature patterns. Koide and Kodera (1999) recently used similar combined fields [from air temperature and GISST datasets described by Jones et al. (1999)] and found some association with 500-hPa variability. Our merged fields allow us to estimate the gradients of surface temperatures, which were computed for each grid point taking into account the latitudinal convergence. Figure 12a shows the magnitudes and directions of climatological winter surface gradients for the northwest Atlantic area 30°–58°N, 90°–25°W. The strongest gradients are observed over the North American coast where they are approximately 1.5 times larger than for the oceanic SST front. Over the American continent the gradients are of somewhat smaller magnitude and align nearly zonally from the Atlantic along the northern coast of the Great Lakes.

Since the directions of the mean surface temperature gradients remain very stable (the largest range of interannual variability is $\pm 10°$), we applied EOF analysis

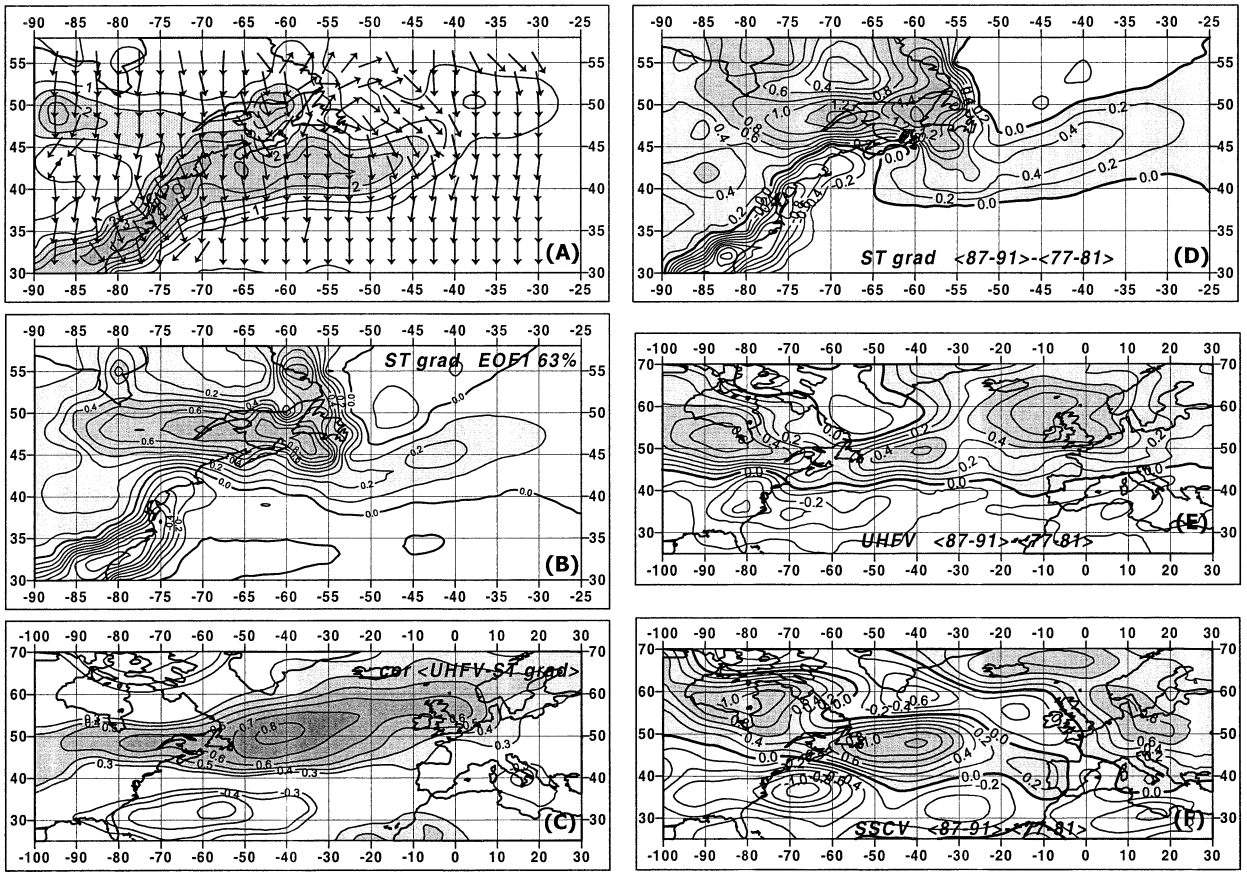

FIG. 12. (a) Magnitudes [°C (100 km)$^{-1}$] and directions of surface temperature gradients in the northwest Atlantic area, (b) first EOF of surface temperature gradient, (c) associated correlations between the first principal component of surface temperature gradient and UHFV, (d) differences between the periods 1987–91 and 1977–81 for the surface temperature gradients [°C (100 km)$^{-1}$], (e) UHFV of the thickness of 1000–500-hPa layer, and (f) SSCV of 500-hPa height.

to the anomalies of the gradient magnitudes. The first EOF of the anomalies of the gradient (Fig. 12b) accounts for 63% of the total variance. It is characterized by the dipole made by the gradients over the North American coast and by the SST gradients at the subpolar front. This goes hand in hand with the surface gradients over the subpolar North American continent. Dickson and Namias (1976) found out-of-phase behavior between the ''coastal'' and ''Great Lakes'' surface temperature gradients. Figure 12 shows that the Great Lakes pattern is highly correlated with midlatitudinal SST gradients. Sharp surface temperature gradients can be associated with local intensification of the baroclinic instability in the lower troposphere, connected with the anomalous surface energy exchange. Rapidly intensifying cyclones are primarily associated with the coastline of the American continent (Sanders 1986; Rogers and Bosart 1986). Yau and Jean (1989) showed that the generation of very fast and deep cyclones in the North Atlantic occurs over either the American coastal zone, or over the Gulf Stream SST front. Hoskins and Valdes (1990) argued that the diabatic heating is very important for the maintenance of baroclinicity. Figure 13 shows that the first principal components of the surface temperature gradient and UHFV are highly correlated ($r = 0.83$), although the correlation with PC1 of the intensity of SSCV is not as high ($r = 0.62$). Figure 12c shows the associated correlation between the first principal component of the surface temperature gradient and the intensity of UHFV. The pattern of associated correlation resembles nearly one to one the first EOF of UHFV. Thus, variability of the local temperature gradients between the subtropical Atlantic and the American continent on one hand, and at the subpolar SST front and over Canada on the other, is closely connected with the intensity of the high-frequency atmospheric synoptic processes. This may represent a driving mechanism through the increase of baroclinic instability of the lower troposphere. Consideration of surface temperature gradients is more effective in comparison to the surface temperatures themselves. EOF analysis of surface temperatures (not shown here) indicates a weakly pronounced land–sea pattern of the second EOF (10% of variance), while the south–north pattern presented by the first EOF is responsible for 52% of total variance,

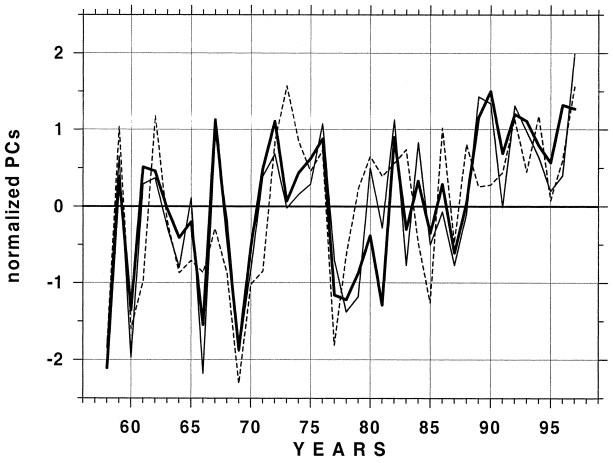

FIG. 13. First normalized principal component of surface temperature gradient (bold line) and recalled from Fig. 9a first normalized principal components of UHFV (thin line) and SSCV (dashed line).

which is similar to the results of Koide and Kodera (1999).

Figure 12e shows differences in the intensity of UHVF in the thickness of the 1000–500-hPa layer between the 5-yr periods 1987–91 and 1977–81. These correspond to the strongest positive and negative anomalies of the surface temperature gradients (Fig. 12d). Strong intensification of UHFV over the whole midlatitudinal storm track is associated with the increase of surface temperature gradients at the subpolar SST front and over the American continent [0.5°–1.5°C (100 km)$^{-1}$] and a strong decrease of local sea–land gradients over the U.S. coast [0.8°–2°C (100 km)$^{-1}$]. However, changes in the intensity of SSCV (Fig. 12f), are negative in the area of the midlatitudinal storm track. Note the remarkable disagreement between the surface temperature gradient and the intensity of synoptic transients in the late 1970s, when there has been a considerable drop of correlation between UHFV and SSCV.

7. Summary and discussion

We described the climatology, trends, and interannual variability of the intensity of synoptic-scale processes in the North Atlantic midlatitudes. Maxima and minima in the intensity of synoptic processes are not collocated for different temporal scales of variability, especially in the lower troposphere. Synoptic processes over the North Atlantic have different interannual and decadal-scale variability patterns for different timescales. The intensities of UHFV and SSCV are highly correlated for the 1960s and early 1970s, but show little relationship with each other in the late 1970s, 1980s, and 1990s. This illustrates the remarkable change in atmospheric variability over the North Atlantic in the late 1970s. This shift is found also in the NAO links to the ice export in the North Atlantic (Hilmer and Jung 2000) and surface temperatures (Kodera et al. 1999). A similar shift has been found in the greenhouse gas experiment with the ECHAM4/OPYC3 coupled model (Ulbrich and Christoph 1999). This may be associated with the intensification of PNJ in the 1980s and 1990s and resulting changes of SSCV in the Atlantic–European sector. During the last 40 yr, UHFV in the North Atlantic has been highly correlated with the anomalies of surface temperature gradient in the Atlantic–American sector. These anomalies exhibit a dipole associated with the U.S. coast, and with the subpolar SST front and continental Canada. This mechanism is primarily pronounced for the fast synoptic processes and the lower troposphere.

The intensities of atmospheric synoptic and subsynoptic variability are closely correlated with each other and with the NAO index during the 1960s and 1970s, but show little consistency during the last two decades. Results in Figs. 11g,h indicate that changes in the intensity of UHFV can be driven by the variability in the lower-troposphere baroclinic instability, while the SSCV may be associated with the hemispheric mode, represented by the PNJ index. In this sense the surface temperature gradient is partly responsible for the changes in the baroclinic instability of the lower atmosphere through the associated local heating. This mechanism is considered in a number of case studies (e.g., Yau and Jean 1989; Giordani and Caniaux 2001). Correlations between the surface temperature gradient and winter SLP anomalies (not shown) are much lower than between the surface temperature gradient and the intensity of UHFV (Fig. 12). From consideration of surface temperature gradients and their close relationships with the intensity of UHFV, we offer a mechanism that is different from the signal traditionally described in terms of SST variability (Zorita et al. 1992; Deser and Blackmon 1993; Kushnir 1994; Venzke et al. 1998; Robertson et al. 2000). Figure 14 shows the first and the second canonical pairs of SST and surface temperature gradients in the northwest Atlantic. The correlation for the first canonical pair is 0.76. The first canonical pattern for the SST resembles to some degree the second EOF of SST associated with the Gulf Stream (Wallace et al. 1990; Deser and Blackmon 1993; others). However, the SST gradient pattern optimally correlated with this SST signal consists of positive anomalies over both the U.S. coast and the subpolar SST front and does not represent the dipole shown in Fig. 12. Only the second canonical pair represents this dipole. Both the SST gradient and SST patterns in this canonical pair closely resemble their respective first EOF patterns. However, the correlation for the second pair is only 0.59. Thus, the signal associated with surface temperature gradients over the northwest Atlantic and North America is different from the traditionally used SST signal.

Variability in the surface temperature gradients in the Atlantic–American sector is represented by the coordinated changes of the SST gradient at the oceanic front and the land–sea temperature differences. Enhancement of the SST gradients may be associated with the bar-

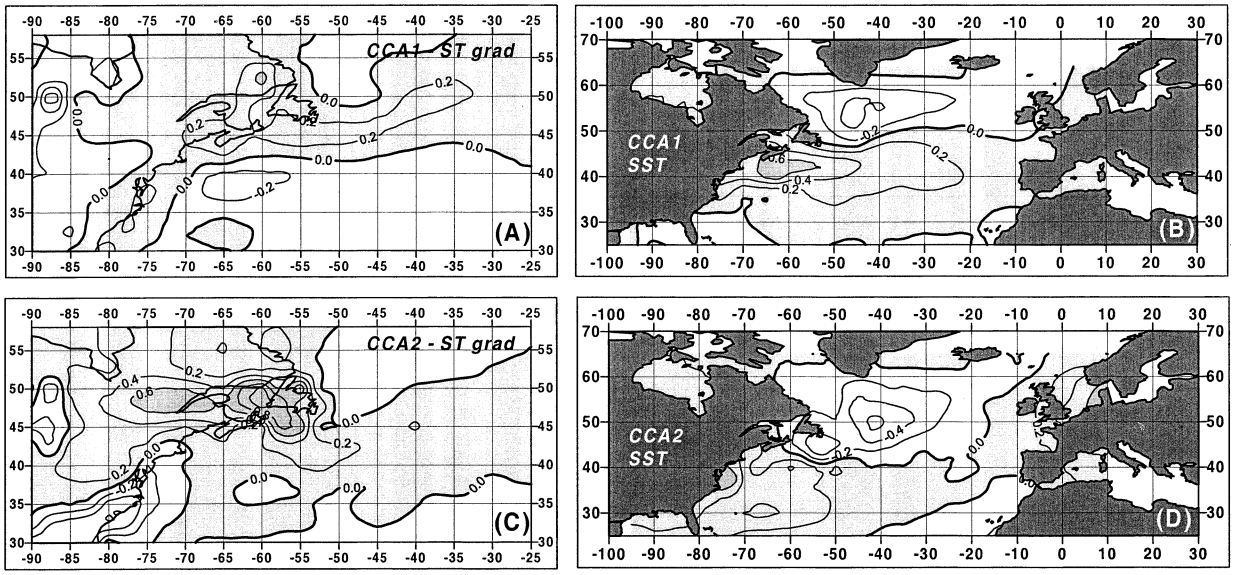

FIG. 14. (a),(b) First and (c),(d) second canonical patterns of (a),(c) surface temperature gradients and (b),(d) sea surface temperatures in the North Atlantic.

oclinic wave response to the heat and momentum forcing in the Labrador Sea. In this case the propagation of the baroclinic boundary waves intensifies following the anomalous density flux in the Labrador Sea (Eden and Willebrand 2001). On the other hand, anomalous density fluxes in the Labrador Sea are closely correlated with the NAO index. In this context, we note that Taylor and Stephens (1998) showed a high correlation between the NAO index and the latitude of the Gulf Stream at an approximate 2-yr lag. Surface temperatures over the continent are reasonably less persistent than the SST. In this sense, it is reasonable to question the degree to which changes in the continental surface temperatures can be influenced by the advection of atmospheric air masses. This feedback issue can be better answered using the results of coupled model experiments.

An important issue is how the surface temperature gradients are linked to the atmospheric circulation during different winter months. Peng and Fyfe (1996) and Ting and Peng (1995) found that the coupling between the SST pattern and the leading SLP mode in the North Atlantic changed slightly from one winter month to another. In this context it would be interesting to consider the relationships between UHFV and SSCV under the intermediate Greenland anticyclone and Atlantic ridge regimes. Although these regimes are sometimes hardly detectable (e.g., Smyth et al. 1999), they may be partly responsible for the complex relationships between the intensity of synoptic-scale transients and their subsynoptic counterpart. An important task is to link the changes in the intensity of atmospheric synoptic processes on different scales, derived from the bandpass statistics, with the characteristics of the cyclone life cycle. Recently Gulev et al. (2001) and Geng and Sugi (2001) found pronounced decadal changes in the cyclone intensity, deepening rate, and propagation velocity. Another avenue for further research is to examine surface ocean–atmosphere fluxes. These may be more effective than the SSTs in characterizing the surface ocean signal and can account partly for the surface temperature gradient mode. Relationships between SST, surface flux, and atmospheric circulation patterns were studied by Cayan (1992a,b) and Iwasaka and Wallace (1995). However, before revisiting this issue, the reliability of ocean–atmosphere fluxes from different sources (including reanalyses) has to be addressed. Surface fluxes in the northwest Atlantic are strongly affected by space–time synoptic variability and averaging effects (Gulev 1994, 1997b) have to be accounted for. A quantitative description of the variability in the intensity of atmospheric synoptic processes of different scales can help to understand the mechanisms of the changes of ocean surface parameters. In particular, observed changes in the North Atlantic wave height (Bacon and Carter 1991, 1993; Kushnir et al. 1997; Gulev and Hasse 1999) can be influenced not only by the wind forcing magnitude but also by forcing frequency.

Acknowledgments. We thank our colleagues Rolf Juerrens, Rolf Fuhrhop, Michael Hilmer, and Oliver Timm for the useful discussions and help in our work. We thank Anne Meyer whose everyday job was very important for us. We appreciate the support of the IFM computer center staff, particularly Kai Grunau. Special thanks to Roland Schweitzer of CDC (Boulder, Colorado), Glenn White of NCEP (Camp Springs, Maryland), and Chi-Fan Chih and Steve Worley of NCAR (Boulder, Colorado), who made available the NCEP–NCAR reanalysis data for us and helped us to resolve numerous problems with the access to these data. We

thank both anonymous reviewers, whose suggestions and criticism helped to improve the manuscript. This work is supported by the Deutsche Forschungsgemeinschaft Sonderforschungsbereich SFB-460, Volkswagen Stiftung (Hannover, Germany) through the project ''North Atlantic Oscillation: Regional Impacts on European Weather and Climate,'' and the Russian Foundation for Basic Research (Grant 64-656).

APPENDIX

Validation of the Bandpass Statistics and Analysis of Sensitivity to Different Filtering Procedures

The reliability of our results warrants discussion. Although the NCEP–NCAR reanalysis used a frozen data assimilation system, it might be influenced by changes in the amount and quality of assimilation data. White (1999) found trends in some basic variables to be dependent on the changes in the number of observations assimilated. This problem is especially important over the ocean where there was a definite break in the number of upper-layer observations in the mid-1970s when observations from most of the North Atlantic Ocean Weather Ships (OWS) were terminated. We compared the intensities of synoptic processes from the NCEP–NCAR reanalysis with similar estimates derived from the OWS data. Twice-daily radiosonde ascents at OWSs A, B, D, I, and J are available from the NCDC from the early 1950s to the early 1960s, OWSs C and M provide data until 1991 and 1994, respectively, OWS L records span 1976–94. For the comparison we interpolated the NCEP–NCAR data to the locations of OWSs. Upper-air time series at the OWSs contain gaps for some months, and we excluded seasons with more than 25% missing data. We reproduced in the NCEP–NCAR time series the OWS-like sampling frequency by taking the snapshots only for the UTC times covered by radiosonde data. Then we applied the bandpass filtering to both the OWS and ''undersampled'' NCEP–NCAR reanalysis time series. We did not estimate UHFV because it is poorly sampled by the incomplete 12-hourly time series. Table A1 shows the results of the regression analysis for the winter season for eight locations in the North Atlantic. Intensities of synoptic processes computed from the NCEP–NCAR reanalysis agree well with those derived from the OWS data. This is not surprising, as this intercomparison is not independent because OWS data were assimilated by the NCEP model. For SSCV there is a tendency for underestimation of high values of std dev and overestimation of low values over the central midlatitudinal North Atlantic. An opposite tendency is obtained for OWS D and M, located in the western Atlantic and Norwegian Sea. Intercepts for SSCV vary within ±5% of the magnitude of climatological values. There is a tendency for overestimation of SSPV by 3%–6% and underestimation of the intensity of LFV by 5%–10% in the NCEP–NCAR reanalysis data in comparison to OWS data. For low-frequency variability there is a systematic overestimation of high values and underestimation of low values. To assess whether there are any time-dependent biases between the NCEP–NCAR reanalysis and OWS data, we computed orthogonal regression slopes and intercepts for the two periods from 1958 to 1972 and from 1975 to 1994 for the locations of OWSs C, M, and I (1958–72) and C, M, and L (1975–94). OWSs I and L are located within 200 km of each other and we combined these data into one time series. Neither the slopes nor intercepts appreciably change between these two periods, at least for SSCV and SSPV. For both periods the overall regression slopes exceed unity, and the intercepts indicate general overestimation of the NCEP–NCAR std dev by approximately 2% for SSCV and 3% for SSPV. For low-frequency variability there is an overestimation of the NCEP–NCAR reanalysis std dev in comparison to the OWS data in the 1960s by approximately 10% and slight underestimation for the period of 1970s and 1980s. Nevertheless, we can point out that the results from the NCEP–NCAR reanalysis and OWS radiosonde data are in reasonable agreement.

Filtering of the synoptic time series can introduce further uncertainty. To examine this issue we applied (in addition to the Lanczos filter) four alternative filters, which have quite different response functions: running mean (RM), quasi-optimal Tukey filter, Hemming filter, and Murakami (1979) recursive filter. For intercomparison we applied the procedure of ''common EOFs'' de-

TABLE A1. Orthogonal regression slopes and intercepts (dam) for the winter (JFM) std dev of SSCV, SSPV, and LFV of 500-hPa heights from NCEP–NCAR reanalysis and OWS radiosonde data.

OWS	SSCV		SSPV		LFV		No. of seasons
	Slope	Intercept	Slope	Intercept	Slope	Intercept	
A	0.963	−0.27	0.949	0.43	1.045	−0.84	12
B	0.988	−0.34	0.991	0.28	1.038	−1.11	13
C	0.995	0.09	1.008	0.51	1.043	−1.24	36
D	1.034	−0.19	1.029	0.34	1.021	−0.76	9
I	1.003	0.11	1.025	0.09	1.029	−0.69	10
J	0.951	−0.16	0.963	0.21	1.009	−0.89	14
L	0.996	0.49	0.984	0.19	1.018	−1.54	16
M	1.029	−0.19	1.031	0.39	1.033	1.92	31

TABLE A2. Partial eigenvalues for the leading modes of the winter UHFV and SSCV computed using different filtering operations.

Mode No.	1		2		3	
Filter	UHFV	SSCV	UHFV	SSCV	UHFV	SSCV
Lanczos	121.21	279.35	71.44	154.76	34.20	89.93
RM	95.70	209.84	66.42	143.66	41.38	83.47
Tukey	117.54	256.81	65.11	149.77	38.08	79.92
Hemming	99.64	231.70	61.89	135.30	40.03	86.52
Murakami	125.69	276.57	69.56	162.70	35.80	90.10

veloped by Barnett (1999) and aimed to estimate the patterns of variability common to all time series analysed. In general, the five time series derived using different filters demonstrate comparable patterns of variability. This is in agreement with the results of Wallace et al. (1988). Use of the running mean (which has poor spectral characteristics) results in the partial propagation of UHFV to the SSCV range, as well as a smaller spatial shift between the maxima of interannual variability for UHFV and SSCV. When the RM is used, the first two EOFs account for 30% and 19% of total variance for UHFV and for 24% and 17% of total variance for SSCV. The EOFs are not as well separated as for the other filters. The first two common EOFs of UHFV and SSCV are very similar to those shown in Fig. 9 and exhibit magnitudes 5%–10% smaller. The first common EOF accounts for 33% of total variance for the UHFV and for 29% for SSCV. Corresponding percentages for the second EOF are 20% and 18%. Table A2 shows partial eigenvalues for the five space–time series of UHFV and SSCV derived using different filters. The leading EOF dominates in all five space–time series. Murakami (1979) and Lanczos filtering result in a very similar structure of variability. Time series obtained with the use of running mean and Hamming filters demonstrate more variability associated with the highest modes. Thus, the Lanczos window, used in this study, is quite effective for the breakdown of synoptic time series. For the windows with good spectral characteristics, results are insensitive to the filters employed.

REFERENCES

Agee, E. M., 1991: Trends in cyclone and anticyclone frequency and comparison with periods of warming and cooling over the Northern Hemisphere. *J. Climate,* **4,** 263–267.

Akima, H., 1970: A new method of interpolation and smooth curve fitting based on local procedures. *J. Appl. Comput. Math.,* **17,** 589–602.

Alpert, P. B., U. Neeman, and Y. Shau-El, 1990: Interannual variability of cyclone tracks in the Mediterranean. *J. Climate,* **3,** 1474–1478.

Ayrault, F., F. Lalaurette, A. Joly, and C. Loo, 1995: North Atlantic ultra high frequency variability. *Tellus,* **47A,** 671–696.

Bacon, S., and D. J. T. Carter, 1991: Wave climate changes in the North Atlantic and North Sea. *Int. J. Climatol.,* **11,** 545–588.

——, and ——, 1993: A connection between mean wave height and atmospheric pressure gradient in the North Atlantic. *Int. J. Climatol.,* **13,** 423–436.

Barnett, T. P., 1999: Comparison of near-surface air temperature variability in 11 coupled global climate models. *J. Climate,* **12,** 511–518.

Barnston, A. G., and R. E. Livezey, 1987: Classification, seasonality and persistence of low-frequency atmospheric circulation patterns. *Mon. Wea. Rev.,* **115,** 1083–1126.

Battisti, D. S., U. S. Bhatt, and M. A. Alexander, 1995: A modeling study of the interannual variability in the wintertime North Atlantic Ocean. *J. Climate,* **8,** 3067–3083.

Bjerknes, J., 1964: Atlantic air–sea interaction. *Advances in Geophysics,* Vol. 10, Academic Press, 1–82.

Blackmon, M. L., Y. H. Lee, J. M. Wallace, and H. H. Hsu, 1984: Horizontal structure of 500 mb height fluctuations with long, intermediate and short time scales. *J. Atmos. Sci.,* **41,** 961–979.

Blender, R., K. Fraedrich, and F. Lunkeit, 1997: Identification of cyclone track regimes in the North Atlantic. *Quart. J. Roy. Meteor. Soc.,* **123,** 727–741.

Branstator, G., 1995: Organization of storm track anomalies by recurring low-frequency circulation anomalies. *J. Atmos. Sci.,* **52,** 207–226.

Broccoli, A. J., N.-C. Lau, and M. J. Nath, 1998: The cold ocean–warm land pattern: Model simulation and relevance to climate change detection. *J. Climate,* **11,** 2743–2763.

Cayan, D., 1992a: Variability of latent and sensible heat fluxes estimated using bulk formulae. *Atmos.–Ocean,* **30,** 1–42.

——, 1992b: Latent and sensible heat flux anomalies over the northern oceans: The connection to monthly atmospheric circulation. *J. Climate,* **5,** 354–369.

Christoph, M., U. Ulbrich, and P. Speth, 1997: Midwinter suppression of Northern Hemisphere storm track activity in the real atmosphere and in GCM experiments. *J. Atmos. Sci.,* **54,** 1589–1599.

da Silva, A. M., and G. White, 1996: Intercomparison of surface marine fluxes from GEOS, NCEP/NCAR and ERA Reanalyses and COADS. *Proc. WCRP Workshop on Air–Sea Flux Fields from Forcing Ocean Models and Validating GCMs,* Reading, United Kingdom, World Meteorological Organization, WMO/TD-762, 19–24.

Davis, R. E., B. R. Hayden, D. A. Gay, W. L. Phillips, and G. V. Jones, 1997: The North Atlantic subtropical anticyclone. *J. Climate,* **10,** 728–744.

Deser, C., and M. L. Blackmon, 1993: Surface climate variations over the North Atlantic Ocean during winter: 1900–1989. *J. Climate,* **6,** 1743–1753.

Dickson, R. R., and J. Namias, 1976: North American influences on the circulation and climate of the North Atlantic sector. *Mon. Wea. Rev.,* **104,** 1255–1265.

Duchon, C. E., 1979: Lanczos filtering in one and two dimensions. *J. Appl. Meteor.,* **18,** 1016–1022.

Eden, C., and J. Willebrand, 2001: Mechanism of interannual to decadal variability of the North Atlantic circulation. *J. Climate,* **14,** 2266–2280.

Geng, Q., and M. Sugi, 2001: Variability of the North Atlantic cyclone activity in winter analyzed from NCEP–NCAR reanalysis data. *J. Climate,* **14,** 3863–3873.

Gibson, J. K., P. Kallberg, S. Uppala, A. Nomura, A. Hernandes, and A. Serrano, 1997: ERA description. ECMWF Reanalysis Project Report Series 1, 77 pp.

Giordani, H., and G. Caniaux, 2001: Sensitivity of cyclogenesis to

sea surface temperature in the northwestern Atlantic. *Mon. Wea. Rev.*, **129,** 1273–1295.
Glowienska-Hense, R., 1990: Oscillations in the Atlantic–European SLP. *Tellus*, **42A,** 497–507.
Groetzner, A., M. Latif, and T. P. Barnett, 1998: A decadal climate cycle in the North Atlantic Ocean as simulated by the ECHO coupled GCM. *J. Climate,* **11,** 831–847.
Gulev, S. K., 1994: Influence of space–time averaging on the ocean–atmosphere exchange estimates in the North Atlantic midlatitudes. *J. Phys. Oceanogr.*, **24,** 1236–1255.
——, 1997a: Climate variability of the intensity of synoptic processes in the North Atlantic midlatitudes. *J. Climate,* **10,** 574–592.
——, 1997b: Climatologically significant effects of space–time averaging in the North Atlantic sea–air heat flux fields. *J. Climate,* **10,** 2743–2763.
——, and L. Hasse, 1999: Changes of wind waves in the North Atlantic over the last 30 years. *Int. J. Climatol.*, **19,** 720–744.
——, O. Zolina, and S. Grigoriev, 2001: Extratropical cyclone variability in the Northern Hemisphere winter from the NCEP/NCAR Reanalysis data. *Climate Dyn.*, **17,** 795–810.
Halliwell, G. R., 1997: Decadal and multidecadal North Atlantic SST anomalies driven by standing and propagating basin-scale atmospheric anomalies. *J. Climate,* **10,** 2405–2411.
——, and D. A. Mayer, 1996: Frequency response properties of forced climatic SST anomaly variability in the North Atlantic. *J. Climate,* **9,** 3576–3587.
Hannachi, A., and B. Legras, 1995: Simulated annealing and weather regimes classification. *Tellus*, **47A,** 955–973.
Harnack, R. P., and A. J. Broccoli, 1979: Associations between sea surface temperature gradient and overlying midtropospheric circulation in the North Pacific region. *J. Phys. Oceanogr.*, **9,** 1232–1242.
Hense, A., R. Glowienka-Hense, and H. von Storch, 1990: Northern Hemisphere atmospheric response to changes of the Atlantic Ocean SST on decadal time scales. *Climate Dyn.*, **4,** 157–174.
Heyen, H., E. Zorita, and H. von Storch, 1996: Statistical downscaling of monthly mean North Atlantic air-pressure to sea-level anomalies in the Baltic Sea. *Tellus*, **48A,** 312–323.
Hilmer, M., and T. Jung, 2000: Evidence for a recent change in the link between the North Atlantic Oscillation and Arctic sea ice. *Geophys. Res. Lett.*, **27,** 989–992.
Hoskins, B. J., and P. D. Sardeshmukh, 1987: Transient eddies and the seasonal mean rotational flow. *J. Atmos. Sci.*, **44,** 328–338.
——, and P. J. Valdes, 1990: On the existence of storm tracks. *J. Atmos. Sci.*, **47,** 1854–1864.
——, and K. I. Hodges, 2002: New perspectives on the Northern Hemisphere winter storm tracks. *J. Atmos. Sci.*, **59,** 1041–1061.
——, I. N. James, and G. H. White, 1983: The shape, propagation and mean flow interaction of large scale weather systems. *J. Atmos. Sci.*, **40,** 1595–1612.
Hurrell, J. W., 1995a: Transient eddy forcing of the rotational flow during northern winter. *J. Atmos. Sci.*, **52,** 2286–2300.
——, 1995b: Decadal trends in the North Atlantic Oscillation: Regional temperatures and precipitation. *Science,* **269,** 676–679.
——, 1996: Influence of variations in extratropical wintertime teleconnections on Northern Hemisphere temperature. *Geophys. Res. Lett.*, **23,** 665–668.
——, and H. van Loon, 1997: Decadal variations on climate associated with the North Atlantic Oscillation. *Climatic Change,* **36,** 301–326.
Iwasaka, N., and J. M. Wallace, 1995: Large-scale air–sea interaction in the Northern Hemisphere from a view point of variations of surface heat flux by SVD analysis. *J. Meteor. Soc. Japan,* **73,** 781–794.
Jones, P. D., M. New, D. E. Parker, S. Martin, and I. G. Rigor, 1999: Surface air temperature and its changes over the past 150 years. *Rev. Geophys.*, **37,** 173–199.
Kalnay, E., and Coauthors, 1996: The NCEP/NCAR 40-Year Reanalysis Project. *Bull. Amer. Meteor. Soc.*, **77,** 437–471.
Kodera, K., H. Koide, and H. Yoshimura, 1999: Northern Hemisphere winter circulation associated with the North Atlantic Oscillation and stratospheric polar night jet. *Geophys. Res. Lett.*, **26,** 443–446.
Koide, H., and K. Kodera, 1999: A SVD analysis between the winter NH 500-hPa height and surface temperature fields. *J. Meteor. Soc. Japan,* **77,** 47–61.
Kushnir, Y., 1994: Interdecadal variations in North Atlantic sea surface temperature and associated atmospheric conditions. *J. Climate,* **7,** 141–157.
——, V. J. Cardone, J. G. Greenwood, and M. A. Cane, 1997: The recent increase in the North Atlantic wave height. *J. Climate,* **10,** 2107–2113.
Lambert, S., 1996: Intense extratropical Northern Hemisphere winter cyclone events: 1899–1991. *J. Geophys. Res.*, **101,** 21 319–21 325.
Lanczos, C., 1956: *Applied Analysis.* Prentice-Hall, 539 pp.
Lanzante, J. R., 1983: A further assessment of the association between sea surface temperature gradient and the overlying midtropospheric circulation. *J. Phys. Oceanogr.*, **13,** 1971–1974.
Latif, M., and T. P. Barnett, 1994: Causes of decadal variability over the North Pacific and North America. *Science,* **266,** 634–637.
Liu, Q., and T. Opsteegh, 1995: Interannual and decadal variations of blocking activity in a quasi-geostrophic model. *Tellus,* **47A,** 941–954.
Maechel, H., A. Kapala, and H. Flohn, 1998: Behavior of the centres of action above the Atlantic since 1881. Part I: Characteristics of seasonal and interannual variability. *Int. J. Climatol.*, **18,** 1–22.
Murakami, M., 1979: Large-scale aspects of deep convective activity over the GATE area. *Mon. Wea. Rev.*, **107,** 994–1013.
Peng, S., and J. Fyfe, 1996: The coupled patterns between sea level pressure and sea surface temperature in the midlatitude North Atlantic. *J. Climate,* **9,** 1824–1839.
Robertson, A. W., and W. Metz, 1990: Transient eddy feedbacks derived from linear theory and observations. *J. Atmos. Sci.*, **47,** 929–950.
——, C. R. Mechoro, and Y.-J. Kim, 2000: The influence of Atlantic sea surface temperature anomalies on the North Atlantic oscillation. *J. Climate,* **13,** 122–138.
Rodwell, M. J., D. P. Rowell, and C. K. Folland, 1999: Oceanic forcing of the wintertime North Atlantic Oscillation and European climate. *Nature,* **398,** 320–323.
Rogers, E., and L. F. Bosart, 1986: An investigation of explosively deepening oceanic cyclones. *Mon. Wea. Rev.*, **114,** 702–718.
Rogers, J. C., 1984: The association between the North Atlantic Oscillation and the Southern Oscillation in the Northern Hemisphere. *Mon. Wea. Rev.*, **112,** 1999–2015.
——, 1997: North Atlantic storm track variability and its association to the North Atlantic oscillation and climate variability of northern Europe. *J. Climate,* **10,** 1635–1647.
Sanders, F., 1986: Explosive cyclogenesis in the west-central North Atlantic Ocean, 1981–84. Part I: Composite structure and mean behavior. *Mon. Wea. Rev.*, **114,** 1781–1794.
Schinke, H., 1993: On the occurrence of deep cyclones over Europe and the North Atlantic in the period 1930–1991. *Beitr. Phys. Atmos.*, **66,** 223–237.
Serreze, M. C., F. Carse, R. G. Barry, and J. C. Rogers, 1997: Icelandic low cyclone activity: Climatological features, linkages with the NAO, and relationships with recent changes in the Northern Hemisphere circulation. *J. Climate,* **10,** 453–464.
Simmons, A., and B. J. Hoskins, 1978: Life cycles of some nonlinear baroclinic waves. *J. Atmos. Sci.*, **35,** 414–432.
Smith, T. M., R. W. Reynolds, R. E. Livezey, and D. S. Stokes, 1996: Reconstruction of historical sea surface temperatures using empirical orthogonal functions. *J. Climate,* **9,** 1403–1420.
Smyth, P., K. Ide, and M. Ghil, 1999: Multiply regimes in the Northern Hemisphere height fields via mixture model clustering. *J. Atmos. Sci.*, **56,** 3704–3723.
Stein, O., and A. Hense, 1994: A reconstructed time series of the

number of extreme low pressure events since 1880. *Meteor. Z.,* **3,** 43–46.
Stephenson, D. B., V. Pavan, and R. Bojariu, 2000: Is the North Atlantic Oscillation a random walk? *Int. J. Climatol.,* **20,** 1–18.
Sutton, R. T., and M. R. Allen, 1997: Decadal predictability of the North Atlantic sea surface temperature and climate. *Nature,* **388,** 563–567.
Taylor, A. H., and J. A. Stephens, 1998: North Atlantic Oscillation and the latitude of the Gulf Stream. *Tellus,* **50A,** 134–142.
Thompson, D. W., and J. M. Wallace, 1998: The Arctic Oscillation signature in the wintertime geopotential height and temperature fields. *Geophys. Res. Lett.,* **25,** 1297–1300.
Ting, M., and S. Peng, 1995: Dynamics of the early and middle winter atmospheric responses to the northwest Atlantic SST anomalies. *J. Climate,* **8,** 2239–2254.
Trenberth, K. E., 1991: Storm tracks in the Southern Hemisphere. *J. Atmos. Sci.,* **48,** 2159–2178.
——, and D. A. Paolino, 1980: The Northern Hemisphere sea-level pressure data set: Trends, errors and discontinuities. *Mon. Wea. Rev.,* **108,** 855–872.
Ueno, K., 1993: Interannual variability of surface cyclone tracks, atmospheric circulation patterns, and precipitation patterns in winter. *J. Meteor. Soc. Japan,* **71,** 655–671.
Ulbrich, U., and M. Christoph, 1999: A shift of the NAO and increasing storm track activity over Europe due to anthropogenic greenhouse gas forcing. *Climate Dyn.,* **15,** 551–559.
van Loon, H., and J. C. Rogers, 1978: The seesaw in winter temperatures between Greenland and Northern Europe. Part I: General description. *Mon. Wea. Rev.,* **106,** 296–310.
Venzke, S., M. R. Allen, R. T. Sutton, and D. P. Rowell, 1998: The atmospheric response over the North Atlantic to decadal changes in sea surface temperature. Max-Planck-Institut für Meteorologie Rep. 255, Hamburg, Germany, 46 pp.
von Storch, H., and F. W. Zwiers, 1999: *Statistical Analysis in Climate Research.* Cambridge University Press, 503 pp
——, and Coauthors, 1993a: Changing statistics of storms in the North Atlantic. Max-Planck-Institut für Meteorologie Rep. 116, Hamburg, Germany, 19 pp.
——, E. Zorita, and U. Cubasch, 1993b: Downscaling of global climate change estimates to regional scales: An application to Iberian rainfall in wintertime. *J. Climate,* **6,** 1161–1171.
Wallace, J. M., G.-H. Lim, and M. Blackmon, 1988: Relationship between cyclone tracks, anticyclone tracks and baroclinic waveguides. *J. Atmos. Sci.,* **45,** 439–462.
——, C. Smith, and Q. Jiang, 1990: Spatial patterns of atmosphere–ocean interaction in the northern winter. *J. Climate,* **3,** 990–998.
——, ——, and C. S. Bretherton, 1992: Singular value decomposition of wintertime sea surface temperature and 500-mb height anomalies. *J. Climate,* **5,** 561–576.
——, Y. Zhang, and J. A. Renwick, 1995: Dynamic contribution to hemispheric mean temperature trends. *Science,* **270,** 780–783.
White, G., 1999: Long-term trends in the NCEP/NCAR Reanalysis. *Proc. Second Int. Conf. on Reanalyses,* Reading, United Kingdom, World Meteorological Organization WCRP-109 (WMO/TD985), 54–57.
Woodruff, S. D., H. F. Diaz, J. D. Elms, and S. J. Worley, 1998: COADS Release 2 data and metadata enhancements for improvements of marine surface flux fields. *Phys. Chem. Earth,* **23,** 517–526.
Yau, M. K., and M. Jean, 1989: Synoptic aspects and physical processes in the rapidly intensifying cyclone of 6–8 March 1986. *Atmos.–Ocean,* **27,** 59–86.
Zorita, E., V. Kharin, and H. von Storch, 1992: The atmospheric circulation and sea surface temperature in the North Atlantic area in winter: Their interaction and relevance for Iberian precipitation. *J. Climate,* **5,** 1097–1108.